Computer Modeling in Engineering & Sciences

Tech Science Press

Doi:10.32604/cmes.2025.063971

ARTICLE

Numerical Treatments for a Crossover Cholera Mathematical Model Combining Different Fractional Derivatives Based on Nonsingular and Singular Kernels

Seham M. AL-Mekhlafi[1,*], Kamal R. Raslan[2], Khalid K. Ali[2], Sadam. H. Alssad[2,3] and Nehaya R. Alsenaideh[4]

[1]Department of Mathematics, Faculty of Education, Sana'a University, Sana'a, 1247, Yemen
[2]Mathematics Department, Faculty of Science, Al-Azhar University, Nasr-City, Cairo, 11651, Egypt
[3]Mathematics Department, Faculty of Education, Abyan University, Abyan, Yemen
[4]Ain Shams University Mathematics Department, Faculty of Science, Ain Shams University, Cairo, 11566, Egypt

*Corresponding Author: Seham M. AL-Mekhlafi. Email: sih.almikhlafi@su.edu.ye

Received: 30 January 2025; Accepted: 07 April 2025; Published: 30 May 2025

ABSTRACT: This study introduces a novel mathematical model to describe the progression of cholera by integrating fractional derivatives with both singular and non-singular kernels alongside stochastic differential equations over four distinct time intervals. The model incorporates three key fractional derivatives: the Caputo-Fabrizio fractional derivative with a non-singular kernel, the Caputo proportional constant fractional derivative with a singular kernel, and the Atangana-Baleanu fractional derivative with a non-singular kernel. We analyze the stability of the core model and apply various numerical methods to approximate the proposed crossover model. To achieve this, the approximation of Caputo proportional constant fractional derivative with Grünwald-Letnikov nonstandard finite difference method is used for the deterministic model with a singular kernel, while the Toufik-Atangana method is employed for models involving a non-singular Mittag-Leffler kernel. Additionally, the integral Caputo-Fabrizio approximation and a two-step Lagrange polynomial are utilized to approximate the model with a non-singular exponential decay kernel. For the stochastic component, the Milstein method is implemented to approximate the stochastic differential equations. The stability and effectiveness of the proposed model and methodologies are validated through numerical simulations and comparisons with real-world cholera data from Yemen. The results confirm the reliability and practical applicability of the model, providing strong theoretical and empirical support for the approach.

KEYWORDS: Cholera crossover model; Caputo proportional constant fractional derivative; Caputo-Fabrizio fractional derivative; Atangana Baleanu fractional derivative; stochastic differential equations (SDE)

1 Introduction

Cholera continues to pose a major public health challenge, particularly in endemic regions where sanitation and access to clean water are limited. According to Ali et al. [1], cholera remains a significant burden in many parts of the world, with periodic outbreaks contributing to considerable morbidity and mortality. Mathematical modeling has become an essential tool in understanding and predicting the spread of infectious diseases like cholera, offering insights that inform public health interventions and optimize resource allocation. Huppert and Katriel [2] emphasize the importance of mathematical frameworks in epidemiology, highlighting their capacity to simulate complex transmission dynamics and forecast outbreak patterns.

Recent advancements in mathematical modeling have incorporated fractional calculus to better represent the memory effects and hereditary properties inherent in disease transmission. Fractional-order models provide a more flexible and accurate description of epidemic processes compared to classical integer-order models, capturing the influence of past states on current disease progression. Lemos-Paião et al. [3] developed a cholera model with optimal control strategies, demonstrating how fractional dynamics can significantly enhance our understanding of disease spread and control measures. Similarly, the work by Lemos-Paião et al. [4] introduced an epidemic model for cholera that utilizes optimal control to manage treatment strategies, further illustrating the utility of fractional models in epidemiological applications.

Baleanu et al. [5] expanded on these approaches by proposing a generalized fractional model for real cholera outbreaks, incorporating stochastic components to account for the unpredictable nature of disease dynamics. Their model successfully captured the complexities observed in actual outbreaks, validating the effectiveness of fractional and stochastic approaches in improving predictive accuracy.

Fractional calculus has gained significant attention in recent years due to its ability to describe memory effects and hereditary properties in various physical and biological systems. Unlike classical integer-order derivatives, fractional derivatives provide a more generalized framework for modeling complex dynamical processes. In particular, special functions play a crucial role in solving fractional differential equations, offering analytical and numerical tools for applications in engineering, physics, and mathematical biology. The work presented in [6] explores the fundamental role of special functions in fractional models, highlighting their applicability in diverse scientific domains. Incorporating these special functions allows for more accurate representations of anomalous diffusion, viscoelastic materials, and population dynamics. This perspective aligns with our study, where fractional-order derivatives are employed to enhance the mathematical modeling of disease transmission and epidemiology, providing deeper insights into system behavior.

Building upon these foundational studies, this paper introduces a novel crossover cholera model that integrates multiple fractional derivatives with both singular and nonsingular kernels, bridging deterministic and stochastic processes to better reflect real-world conditions. The proposed model leverages three distinct types of fractional derivatives:

- Caputo-Fabrizio fractional derivative (nonsingular kernel) [7], known for its smooth memory effects and exponential decay properties.
- Caputo proportional constant fractional derivative (singular kernel) [8], capturing abrupt changes and reflecting more localized influences in the disease dynamics.
- Atangana-Baleanu fractional derivative (nonsingular kernel) [9], offering a more generalized representation of memory effects through Mittag-Leffler functions.

These derivatives are applied across four distinct time intervals, reflecting the various stages of cholera progression, from initial infection to outbreak resolution. By incorporating stochastic differential equations (SDEs) alongside fractional derivatives, the model accounts for the inherent randomness and uncertainty present in disease transmission, environmental factors, and population mobility.

This crossover model not only refines the predictive accuracy of cholera outbreaks but also extends the applicability of fractional calculus to broader epidemiological contexts. By addressing the limitations of traditional models and incorporating stochastic elements, the proposed framework contributes to the ongoing effort to mitigate the global impact of cholera through improved forecasting and intervention strategies.

These derivatives are applied across four distinct time intervals, reflecting the various stages of cholera progression, from initial infection to outbreak resolution. By incorporating stochastic differential equations (SDEs) alongside fractional derivatives, the model accounts for the inherent randomness and uncertainty present in disease transmission, environmental factors, and population mobility.

To ensure accurate numerical approximations, the model employs a combination of advanced numerical techniques:

- The approximation of Caputo proportional constant fractional derivative with Grünwald-Letnikov nonstandard finite difference method (CPC-GLNFDM) is applied to systems with singular kernels to achieve stable and accurate approximations [10].
- The Toufik-Atangana method was utilized for models involving nonsingular Mittag-Leffler kernels, ensuring convergence and minimizing computational error [11].
- Caputo-Fabrizio integral approximation and Lagrange polynomial interpolation applied to nonsingular exponential decay kernels, capturing the long-term behavior of the disease [11].
- The Milstein method is used for stochastic differential equations, providing precise approximations for random fluctuations in transmission dynamics [12].

The authors confirm that this study is original and has not been discussed before, and it is presented in this paper for the first time.

The structure of this study is as follows: Section 2 introduces key definitions of fractional derivatives, provides a brief overview of stochastic differential equations (SDEs), and outlines the numerical methods used to solve them. Section 3 presents the foundational model along with its mathematical analysis. Section 4 introduces a novel crossover model to describe the dynamics of cholera spread. This model integrates three fractional derivatives with both singular and nonsingular kernels, as well as SDEs across four distinct time intervals. The fractional derivatives employed include the Caputo-Fabrizio derivative (nonsingular kernel), the Caputo proportional constant derivative (singular kernel), and the Atangana-Baleanu derivative (nonsingular kernel). Section 5 details the application of four numerical methods to solve the proposed system and analyze its stability. Section 6 presents numerical simulations based on the proposed model, illustrating its performance and accuracy. Section 7 concludes the study by summarizing the key findings and highlighting the primary contributions of the research.

2 Preliminaries and Notations

In this section, we go over some of the most important fractional calculus definitions that are used in the remainder of this research.

Definition 1. *Let* $\Omega = [\mathfrak{a}, \mathfrak{b}]$, *the value of* $\alpha \in \mathbb{C}$, $\Re(\alpha) > 0$, $-\infty < \mathfrak{a} < \mathfrak{b} < \infty$, *reference [13] defines the Riemann-Liouville's derivatives of order* α *on the left and right sides, respectively, for a continuous function* $f(\mathfrak{t})$.

$$ {}_{\mathfrak{a}}D_{\mathfrak{t}}^{\alpha}\mathfrak{f}(\mathfrak{t}) = \frac{1}{\Gamma(-\alpha+\mathfrak{n})}\left(\frac{d}{d\mathfrak{t}}\right)^{\mathfrak{n}}\int_{\mathfrak{a}}^{\mathfrak{t}}\frac{\mathfrak{f}(\mathfrak{s})}{(-\mathfrak{s}+\mathfrak{t})^{\alpha-\mathfrak{n}+1}}d\mathfrak{s}, \quad \mathfrak{t} > \mathfrak{a}, \tag{1} $$

$$ {}_{\mathfrak{t}}D_{\mathfrak{b}}^{\alpha}\mathfrak{f}(\mathfrak{t}) = \frac{1}{\Gamma(-\alpha+\mathfrak{n})}\left(\frac{-d}{d\mathfrak{t}}\right)^{\mathfrak{n}}\int_{\mathfrak{t}}^{\mathfrak{b}}\frac{\mathfrak{f}(\mathfrak{s})}{(-\mathfrak{t}+\mathfrak{s})^{\alpha-\mathfrak{n}+1}}d\mathfrak{s}, \quad \mathfrak{t} < \mathfrak{b}, \tag{2} $$

where $\mathfrak{n} = 1 + [\Re(\alpha)]$.

Definition 2. *Let* $\Omega = [\mathfrak{a}, \mathfrak{b}]$, *the value of* $\alpha \in \mathbb{C}$, $\Re(\alpha) > 0$, $-\infty < \mathfrak{a} < \mathfrak{b} < \infty$. *For a function that is continuous* $\mathfrak{f}(\mathfrak{t})$, *reference [13] defines the Riemann-Liouville's integrals of order* α *on the left and right sides, respectively.*

$$ {}_{\mathfrak{a}}I_{\mathfrak{t}}^{\alpha}\mathfrak{f}(\mathfrak{t}) = \frac{1}{\Gamma(\alpha)}\left[\int_{\mathfrak{a}}^{\mathfrak{t}}\mathfrak{f}(\mathfrak{s})(-\mathfrak{s}+\mathfrak{t})^{-1+\alpha}d\mathfrak{s}\right], \quad \mathfrak{t} > \mathfrak{a}, \tag{3} $$

$$ {}_{\mathfrak{t}}I_{\mathfrak{b}}^{\alpha}\mathfrak{f}(\mathfrak{t}) = \frac{1}{\Gamma(\alpha)}\left[\int_{\mathfrak{t}}^{\mathfrak{b}}\mathfrak{f}(\mathfrak{s})(-\mathfrak{s}+\mathfrak{t})^{-1+\alpha}d\mathfrak{s}\right], \quad \mathfrak{t} < \mathfrak{b}, \tag{4} $$

where $0 < \alpha < 1$.

Definition 3. *Let $\Omega = [\mathfrak{a}, \mathfrak{b}]$, $-\infty < \mathfrak{a} < \mathfrak{b} < \infty$, $\alpha \in \mathbb{C}$ then reference [13] defines the left-side and right-side Caputo's derivatives of order α for a function $f(\mathfrak{t})$, respectively, $f \in AC^n[\mathfrak{a}, \mathfrak{b}]$, i.e., $f^{(k)}$ is absolutely continuous for all $k \leq n$, and $f^{(n)}$ is integrable and $AC^n[\mathfrak{a}, \mathfrak{b}]$ refers to the space of absolutely continuous functions with n derivatives on the interval $[a, b]$.*

$$({}^{C}D^{\alpha}_{a+}\mathfrak{f})(\mathfrak{t}) = ({}^{C}_{a}D^{\alpha}_{\mathfrak{t}}\mathfrak{f})(\mathfrak{t}) = \frac{1}{\Gamma(-\alpha+\mathfrak{n})}\int_{a}^{\mathfrak{t}} \frac{\mathfrak{f}^{(\mathfrak{n})}(\mathfrak{s})}{(-\xi+\mathfrak{t})^{\alpha-\mathfrak{n}+1}}d\mathfrak{s}, \quad \mathfrak{t} > \mathfrak{a}, \tag{5}$$

$$({}^{C}D^{\alpha}_{\mathfrak{b}-}\mathfrak{f})(x) = ({}^{C}_{\mathfrak{t}}D^{\alpha}_{\mathfrak{b}}\mathfrak{f})(\mathfrak{t}) = \frac{(-1)^{\mathfrak{n}}}{\Gamma(\alpha+\mathfrak{n})}\int_{t}^{\mathfrak{b}} \frac{\mathfrak{f}^{(n)}(\mathfrak{s})}{(-\mathfrak{t}+\mathfrak{s})^{\alpha-\mathfrak{n}+1}}d\mathfrak{s}, \quad \mathfrak{t} < \mathfrak{b}. \tag{6}$$

Definition 4. *[8] For $\alpha \in (0,1)$ and $\mathcal{Z}(\mathfrak{t}) \in \mathcal{W}^1_2(0,1)$, the Caputo-Febrizio fractional derivative of $\mathcal{Z}(\mathfrak{t})$ of order α is given by:*

$$0^{CF}D^{\alpha}_{\mathfrak{t}}\mathcal{Z}(\mathfrak{t}) = \frac{\mathcal{N}(\alpha)}{1-\alpha}\int_{0}^{\mathfrak{t}} \frac{d}{d\tau}\mathcal{Z}(\kappa)exp\left[-\frac{\alpha}{1-\alpha}(-\kappa+\mathfrak{t})\right]d\kappa, \tag{7}$$

the normalizing function $\mathcal{N}(\alpha)$ ensures that $\mathcal{N}(0)$ =1 and $\mathcal{N}(1) = 1$. The function $\mathcal{Z}(\mathfrak{t})$'s fractional integral with exponential decay kernel is provided by:

$$0^{CF}D^{\alpha}_{\mathfrak{t}}\mathcal{Z}(\mathfrak{t}) = \frac{1-\alpha}{\mathcal{N}(\alpha)}\mathcal{Z}(t) + \frac{\alpha}{\mathcal{N}(\alpha)}\int_{0}^{\mathfrak{t}} \mathcal{Z}(\kappa)d\kappa, \tag{8}$$

where $\mathcal{W}^1_2(0,1)$ is the Sobolev space of functions with square-integrable first derivatives, $\mathfrak{n} = 1 + [\Re(\alpha)]$, $\Re(\alpha) \notin \mathbb{N}_0$ and $\mathbb{N}_0$ is the set of non-negative integers.

Definition 5. *The Caputo proportional fractional hybrid operator (CP) is generally defined as [8]:*

$$\begin{aligned} {}^{CP}_{0}D^{\alpha}_{\mathfrak{t}}\mathcal{Z}(\mathfrak{t}) &= \left(\int_{0}^{\mathfrak{t}} (\mathcal{G}_1(\mathfrak{s},\alpha)\mathcal{Z}(\mathfrak{s}) + \mathcal{G}_0(\mathfrak{s},\alpha)\mathcal{Z}'(\mathfrak{s}))(-\mathfrak{s}+\mathfrak{t})^{-\alpha}d\mathfrak{s}\right)\frac{1}{\Gamma(-\alpha+1)}, \\ &= (\mathcal{G}_1(\mathfrak{t},\alpha)\mathcal{Z}(\mathfrak{t}) + \mathcal{G}_0(\mathfrak{t},\alpha)\mathcal{Z}'(\mathfrak{t}))\left(\frac{\mathfrak{t}^{-\alpha}}{\Gamma(-\alpha+1)}\right), \end{aligned} \tag{9}$$

where $\mathcal{G}_0(\alpha, t) = \alpha\mathfrak{t}^{(-\alpha+1)}$, $\mathcal{G}_1(\alpha,\mathfrak{t}) = (-\alpha+1)\mathfrak{t}^{\alpha}$, $0 < \alpha < 1$.

Definition 6. *The Caputo proportional constant fractional hybrid operator (CPC) can be defined as [8]:*

$$\begin{aligned} {}^{CPC}_{0}D^{\alpha}_{\mathfrak{t}}\mathcal{Z}(\mathfrak{t}) &= \left(\int_{0}^{\mathfrak{t}} (-\mathfrak{s}+\mathfrak{t})^{-\alpha}(\mathcal{G}_1(\alpha)\mathcal{Z}(\mathfrak{s}) + \mathcal{G}_0(\alpha)\mathcal{Z}'(\mathfrak{s}))d\mathfrak{s}\right)\frac{1}{\Gamma(-\alpha+1)} \\ &= \mathcal{G}_1(\alpha){}^{RL}_{0}I^{1-\alpha}_{\mathfrak{t}}\mathcal{Z}(\mathfrak{t}) + \mathcal{G}_0(\alpha){}^{C}_{0}D^{\alpha}_{\mathfrak{t}}\mathcal{Z}(\mathfrak{t}), \end{aligned} \tag{10}$$

where $\mathcal{G}_0(\alpha) = \alpha\mathcal{T}^{(-\alpha+1)}$, $\mathcal{G}_1(\alpha) = (-\alpha+1)\mathcal{T}^{\alpha}$, $\mathcal{T}$ is a constant.

Definition 7. *According to Caputo, the Atangana Baleanu fractional derivative of the function $\mathcal{Z}(\mathfrak{t})$ is determined by the formula that follows [8]:*

$$0^{ABC}D^{\alpha}_{\mathfrak{t}}\mathcal{Z}(\mathfrak{t}) = \frac{\mathcal{AB}(\alpha)}{-\alpha+1}\int_{a}^{\mathfrak{t}} \dot{\mathcal{Z}}(\kappa)E_{\alpha}[-\frac{\alpha}{-\alpha+1}(-\kappa+\mathfrak{t})^{\alpha}]d\kappa, \tag{11}$$

and the Riemann-Liouville Atangana Baleanu fractional derivative of the function $\mathcal{Z}(\mathfrak{t})$ is determined by the formula that follows:

$$0^{ABR}D_{\mathfrak{t}}^{\alpha}\mathcal{Z}(\mathfrak{t}) = \frac{\mathcal{AB}(\alpha)}{-\alpha+1}\frac{d}{d\tau}\int_a^{\mathfrak{t}}\mathcal{Z}(\kappa)E_{\alpha}[-\frac{\alpha}{-\alpha+1}(-\kappa+\mathfrak{t})^{\alpha}]d\kappa. \tag{12}$$

Here, $\mathcal{AB}(\alpha) = -\alpha+1+\frac{\alpha}{\Gamma(\alpha)}$, $\mathcal{Z}(\mathfrak{t}) \in \mathcal{W}_2^1(0,1)$, and $\alpha \in (0,1)$. The fractional integral is represented by the following equation, which utilizes the Mittag-Leffler kernel:

$$0^{ABC}I_{\mathfrak{t}}^{\alpha}\mathcal{Z}(\mathfrak{t}) = \frac{-\alpha+1}{\mathcal{AB}(\alpha)}\mathcal{Z}(\kappa) + \frac{\alpha}{\mathcal{AB}(\alpha)\Gamma(\alpha)} + \int_0^{\mathfrak{t}}\mathcal{Z}(\kappa)[(-\kappa+\mathfrak{t})^{-1+\alpha}]d\kappa, \tag{13}$$

where $n = 1+[\Re(\alpha)]$, $\Re(\alpha) \notin \mathcal{N}_0$.

Milstein method

SDE can be approximated numerically using the Milstein method in mathematics. It bears the name of Milstein, who published it in 1974 [12]. To solve the following (SDE):

$$d\mathcal{X}(\mathfrak{t}) = dW(\mathfrak{t})g(\mathcal{X}(\mathfrak{t})) + f(\mathcal{X}(\mathfrak{t}))d\mathfrak{t}, \quad \mathcal{X}(0) = \mathcal{X}_0. \tag{14}$$

Using the Milstein method like this:

$$\mathcal{X}^{1+\mathfrak{n}} = \mathcal{X}^{\mathfrak{n}} + f(\mathcal{X}^{\mathfrak{n}})\Delta\mathfrak{t} + \mathfrak{g}(\mathcal{X}^{\mathfrak{n}})\Delta W + 0.5\mathfrak{g}(\mathcal{X}^{\mathfrak{n}})\mathfrak{g}'(\mathcal{X}^{\mathfrak{n}})((\Delta W_{\mathfrak{n}})^2 - \Delta\mathfrak{t}), \tag{15}$$

where $d\Delta W_n$ describes the standard Brownian motion.

3 Model Setup

In this section, we introduce the basic cholera disease model as outlined in [3]. This model incorporates the following fundamental populations: quarantined individuals ($\mathcal{Q}$), infectious individuals ($\mathcal{I}$), susceptible individuals ($\mathcal{S}$), and recovered individuals ($\mathcal{R}$). Additionally, the model considers the population of free bacteria in the environment ($\mathcal{B}$). This inclusion is critical, as cholera transmission occurs when a healthy individual consumes contaminated water containing these bacteria, which are subsequently removed from the aquatic environment.

The parameters of the model are defined in Table 1, and the mathematical representation of the model is presented as follows:

$$\begin{aligned}
\dot{\mathcal{S}}(\mathfrak{t}) &= -\frac{\beta\mathcal{B}(\mathfrak{t})\mathcal{S}(\mathfrak{t})}{\nu+\mathcal{B}(\mathfrak{t})} + \omega\mathcal{R}(\mathfrak{t}) - \mu\mathcal{S}(\mathfrak{t}) + \Lambda,\\
\dot{\mathcal{I}}(\mathfrak{t}) &= \frac{\beta\mathcal{B}(\mathfrak{t})\mathcal{S}(\mathfrak{t})}{\nu+\mathcal{B}(\mathfrak{t})} - (\delta+\mu+\lambda_1)\mathcal{I}(\mathfrak{t}),\\
\dot{\mathcal{Q}}(\mathfrak{t}) &= -(\varepsilon+\mu+\lambda_2)\mathcal{Q}(\mathfrak{t}) + \delta\mathcal{I}(\mathfrak{t}),\\
\dot{\mathcal{R}}(\mathfrak{t}) &= -(\mu+\omega)\mathcal{R}(\mathfrak{t}) + \varepsilon\mathcal{Q}(\mathfrak{t}),\\
\dot{\mathcal{B}}(\mathfrak{t}) &= -\frac{\rho\mathcal{B}(\mathfrak{t})\mathcal{S}(\mathfrak{t})}{\nu+\mathcal{B}(\mathfrak{t})} - d\mathcal{B}(\mathfrak{t}) + \eta\mathcal{I}(\mathfrak{t}).
\end{aligned} \tag{16}$$

3.1 Analysis of the Model

In this study, we assume non-negative initial conditions for system (16):

$$\mathcal{Q}(0) = \mathcal{Q}_0 \geq 0, \quad \mathcal{I}(0) = \mathcal{I}_0 \geq 0, \quad \mathcal{S}(0) = \mathcal{S}_0 \geq 0, \quad \mathcal{R}(0) = \mathcal{R}_0 \geq 0, \quad \mathcal{B}(0) = \mathcal{B}_0 \geq 0.$$

Table 1: Model parameters and initial conditions [3]

Parameter	Description	Value
Λ	Rate of recruitment	$28.4N(0)/365{,}000$ (person daily)
μ	Rate of natural death	1.6×10^{-5} (daily)
β	Rate of swallowing	0.01891 (daily)
ν	Constant of half-saturation	10^7 (cell/mL)
ω	Rate of Immunity waning	0.4/365 (daily)
δ	Rate of isolation	1.15 (daily)
ε	Rate of Recuperation	0.2 (daily)
λ_1	Rate of demise from infection	6×10^{-6} (daily)
λ_2	Rate of demise (in quarantine)	3×10^{-6} (day^{-1})
η	Rate of losing (infected)	10 (cell/mL daily person^{-1})
d	Rate of bacterial death	0.33 (daily)
ρ	Contact rate	0.01891 (cell/mL daily person^{-1})
$\mathcal{S}(0) = \mathcal{S}_0$	Susceptible cases at time zero	28 249 670 (person)
$\mathcal{I}(0) = \mathcal{I}_0$	Infected cases at time zero	750 (person)
$\mathcal{Q}(0) = \mathcal{Q}_0$	Isolated cases at time zero (person)	0 (person)
$\mathcal{R}(0) = \mathcal{R}_0$	Recuperated cases at time zero	0 (person)
$\mathcal{B}(0) = \mathcal{B}_0$	Bacterial density at time zero	275×10^3 (cell/mL)

3.2 Solutions' Boundedness and Positivity

In the following, the domain Ω described in the equations provides the biological constraints and the feasible region for the model variables. Here's the interpretation of each component:

1. Human population domain $\Omega_{\mathcal{H}}$

$$\Omega_{\mathcal{H}} = \left\{ (\mathcal{Q}, \mathcal{I}, \mathcal{S}, \mathcal{R}) \in \mathbb{R}_0^4 : \mathcal{Q}(t) + \mathcal{I}(t) + \mathcal{S}(t) + \mathcal{R}(t) \leq \frac{\Lambda}{\mu} \right\}. \tag{17}$$

Biological Meaning: This constraint ensures that the total population remains within a biologically feasible limit, accounting for recruitment and death rates.

2. Bacterial population domain $\Omega_{\mathcal{B}}$

$$\Omega_{\mathcal{B}} = \left\{ \mathcal{B} \in \mathbb{R}_0^+ : \mathcal{B}(t) \leq \frac{\Lambda \eta}{\mu d} \right\}. \tag{18}$$

Biological Meaning: This constraint reflects the balance between the contribution of bacteria to the environment (from infected individuals) and its natural decay. It ensures that the bacterial population remains within realistic ecological limits.

3. Combined domain Ω

$$\Omega = \Omega_{\mathcal{H}} \times \Omega_{\mathcal{B}}.$$

Biological Meaning: This domain ensures that the model operates within biologically meaningful constraints for both human and bacterial populations.

Lemma 1. *The solutions of system (16) maintain non-negative values for all* $\mathfrak{t} \geq 0$, *provided that the initial conditions (3.1) are non-negative and belong to the non-negative orthant of five-dimensional Euclidean space,* $\mathcal{R}_0^{+5}$.

Proof: We have

$$\begin{cases} \dot{\mathcal{S}}(\mathfrak{t})\Big|_{\xi(\mathcal{S})} = \omega\mathcal{R}(\mathfrak{t}) + \Lambda > 0, \\ \dot{\mathcal{I}}(\mathfrak{t})\Big|_{\xi(\mathcal{I})} = \mathcal{S}(\mathfrak{t})\frac{\mathcal{B}(\mathfrak{t})\beta}{\nu+\mathcal{B}(\mathfrak{t})} > 0, \\ \dot{\mathcal{Q}}(\mathfrak{t})\Big|_{\xi(\mathcal{Q})} = \delta\mathcal{I}(\mathfrak{t}) > 0, \\ \dot{\mathcal{R}}(\mathfrak{t})\Big|_{\xi(\mathcal{R})} = \varepsilon\mathcal{Q}(\mathfrak{t}) > 0, \\ \dot{\mathcal{B}}(\mathfrak{t})\Big|_{\xi(\mathcal{B})} = \eta\mathcal{I}(\mathfrak{t}) > 0, \end{cases}$$

where $\xi(\nu) = \{\nu(\mathfrak{t}) = 0, \nu = \{\mathcal{Q}, \mathcal{I}, \mathcal{S}, \mathcal{R}, \mathcal{B}\}\}$. Therefore, any solution of system (16) is such that $(\mathcal{Q}, \mathcal{I}, \mathcal{S}, \mathcal{R}, \mathcal{B}) \in \mathbb{R}_0^{+5}$ for all $\mathfrak{t} \geq 0$. □

3.3 Analysis of Stability and Equilibrium Points

3.3.1 Equilibrium Points

Equilibrium points represent steady-state conditions where the system remains unchanged over time. In the context of the cholera model, equilibrium points might represent scenarios where the disease has either been eradicated (disease-free equilibrium) or has reached a stable endemic state.

In the context of cholera models, the disease-free equilibrium (DFE) represents a state where the disease has been eradicated from the population.

It is produced when we set the L.H.S. system (16) to zero and put $\mathcal{I} = 0$. We've

$$\mathbf{E}_0 = (\mathcal{Q}_0, \mathcal{I}_0, \mathcal{S}_0, \mathcal{R}_0, \mathcal{B}_0) = \left(0, 0, \frac{\Lambda}{\mu}, 0, 0\right). \tag{19}$$

The endemic equilibrium corresponds to a non-trivial solution where $\mathcal{I} \neq 0$ (i.e., there is a persistent infection in the population). We denote for the endemic equilibrium by $\mathbf{E}^*$ and given as:

$$\mathbf{E}^* = (\mathcal{Q}^*, \mathcal{I}^*, \mathcal{S}^*, \mathcal{R}^*, \mathcal{B}^*).$$

3.3.2 Stability Analysis

First, we compute the fundamental reproduction factor $\mathbf{R}_0$ [14].

Proposition 1: Model (16)'s fundamental reproduction factor is:

$$\mathbf{R}_0 = \frac{\beta\Lambda\eta}{(\delta + \lambda_1 + \mu)(\mu\nu d + \rho\Lambda)}.$$

Proof: Let $\mathcal{F}_i(t)$ represent the rate at which new infections appear in the compartment corresponding to index i [14]. Define $\mathcal{V}_i^+(t)$ as the rate at which individuals enter the compartment associated with index i

through all other means, while $\mathcal{V}_i^-(t)$ denotes the rate at which individuals leave the compartment with index i. Based on this, the matrices $\mathcal{F}(t)$, $\mathcal{V}^+(t)$, and $\mathcal{V}^-(t)$, which are associated with model (16), are given by:

$$\mathcal{F}(\mathrm{t}) = \begin{bmatrix} 0 \\ \dfrac{\beta\mathcal{B}(\mathrm{t})\mathcal{S}(\mathrm{t})}{v+\mathcal{B}(\mathrm{t})} \\ 0 \\ 0 \\ 0 \end{bmatrix}, \quad \mathcal{V}^+(\mathrm{t}) = \begin{bmatrix} \Lambda + \omega\mathcal{R}(\mathrm{t}) \\ 0 \\ \delta\mathcal{I}(\mathrm{t}) \\ \varepsilon\mathcal{Q}(\mathrm{t}) \\ \eta\mathcal{I}(\mathrm{t}) \end{bmatrix}, \quad \mathcal{V}^-(\mathrm{t}) = \begin{bmatrix} \dfrac{\beta\mathcal{B}(\mathrm{t})\mathcal{S}(\mathrm{t})}{v+\mathcal{B}(\mathrm{t})} + \mu\mathcal{S}(\mathrm{t}) \\ \mathfrak{b}_1\mathcal{I}(\mathrm{t}) \\ \mathfrak{b}_2\mathcal{Q}(\mathrm{t}) \\ \mathfrak{b}_3\mathcal{R}(\mathrm{t}) \\ d\mathcal{B}(\mathrm{t}) \end{bmatrix}$$

where:

$$\mathfrak{b}_1 = \delta + \lambda_1 + \mu, \quad \mathfrak{b}_2 = \varepsilon + \lambda_2 + \mu, \quad \mathfrak{b}_3 = \mu + \omega.$$

Thus, since:

$$\mathcal{V}(\mathrm{t}) = \mathcal{V}^-(\mathrm{t}) - \mathcal{V}^+(\mathrm{t}),$$

we have

$$\begin{bmatrix} \mathcal{S}'(\mathrm{t}) \\ \mathcal{I}'(\mathrm{t}) \\ \mathcal{Q}'(\mathrm{t}) \\ \mathcal{R}'(\mathrm{t}) \\ \mathcal{B}'(\mathrm{t}) \end{bmatrix} = \mathcal{F}(\mathrm{t}) - \mathcal{V}(\mathrm{t}).$$

The Jacobian matrix of $\mathcal{F}(\mathrm{t})$ is:

$$F = \begin{bmatrix} 0 & 0 & 0 & 0 & 0 \\ \dfrac{\mathcal{B}(\mathrm{t})\beta}{v+\mathcal{B}(\mathrm{t})} & 0 & 0 & 0 & \dfrac{\mathcal{S}(t)\kappa\beta}{(v+\mathcal{B}(\mathrm{t}))^2} \\ 0 & 0 & 0 & 0 & 0 \\ 0 & 0 & 0 & 0 & 0 \\ 0 & 0 & 0 & 0 & 0 \end{bmatrix}.$$

The Jacobian matrix of $\mathcal{V}(\mathrm{t})$ is:

$$V = \begin{bmatrix} \dfrac{\mathcal{B}(\mathrm{t})\beta}{v+\mathcal{B}(\mathrm{t})} + \mu & 0 & 0 & -\omega & \dfrac{\mathcal{S}(\mathrm{t})\kappa\beta}{(v+\mathcal{B}(\mathrm{t}))^2} \\ 0 & \mathfrak{b}_1 & 0 & 0 & 0 \\ 0 & -\delta & \mathfrak{b}_2 & 0 & 0 \\ 0 & 0 & -\varepsilon & \mathfrak{b}_3 & 0 \\ 0 & -\eta & 0 & 0 & c \end{bmatrix}.$$

Using the disease-free equilibrium $\mathbf{E}_0$ (19), we get the matrices F_0 and V_0 as:

$$F_0 = \begin{bmatrix} 0 & 0 & 0 & 0 & 0 \\ 0 & 0 & 0 & 0 & \frac{\Lambda\beta}{\nu\mu} \\ 0 & 0 & 0 & 0 & 0 \\ 0 & 0 & 0 & 0 & 0 \\ 0 & 0 & 0 & 0 & 0 \end{bmatrix}, \quad V_0 = \begin{bmatrix} \mu & 0 & 0 & -\omega & \frac{\Lambda\beta}{\nu\mu} \\ 0 & \mathfrak{b}_1 & 0 & 0 & 0 \\ 0 & -\delta & \mathfrak{b}_2 & 0 & 0 \\ 0 & 0 & -\varepsilon & \mathfrak{b}_3 & 0 \\ 0 & -\eta & 0 & 0 & c \end{bmatrix}.$$

The model (16)'s fundamental reproduction factor is:

$$\mathbf{R}_0 = \rho\left(F_0 V_0^{-1}\right) = \frac{\beta\Lambda\eta}{(\mu\nu d + \rho\Lambda)(\delta + \lambda_1 + \mu)}.$$

So, the proof is finished. □

Now we prove the disease-free equilibrium $\mathbf{E}_0$'s local stability.

Theorem 2. *The model (16)'s disease-free equilibrium (DFE) $\boldsymbol{E}_0$ is:*

1. *Locally and asymptotically stable, provided that*

$$\Lambda\beta\eta < (\mu\nu d + \rho\Lambda)(\lambda_1 + \delta + \mu).$$

2. *If $\Lambda\beta\eta > (\mu\nu d + \rho\Lambda)(\lambda_1 + \delta + \mu)$, the DFE is unstable.*

Moreover, a critical case arises if:

$$\beta\Lambda\eta = (\mu\nu d + \rho\Lambda)(\delta + \lambda_1 + \mu).$$

Proof: The linearized system of model (16)'s characteristic polynomial is provided by:

$$\tilde{p}(\chi) = \det\left(\mathcal{F}_0 - \mathcal{V}_0 - \mathcal{I}_5\chi\right)$$

To calculate the polynomial p's roots, we possess that

$$\begin{vmatrix} -\chi - \mu & 0 & 0 & \omega & -\frac{\Lambda\beta}{\kappa\mu} \\ 0 & -\chi - \mathfrak{b}_1 & 0 & 0 & \frac{\Lambda\beta}{\nu\mu} \\ 0 & \delta & -\chi - \mathfrak{b}_2 & 0 & 0 \\ 0 & 0 & \varepsilon & -\chi - \mathfrak{b}_3 & 0 \\ 0 & \eta & 0 & 0 & -\chi - d \end{vmatrix} = 0.$$

That is:

$$\chi = -\mu, \quad \chi = -\mathfrak{b}_2, \quad \chi = -\mathfrak{b}_3, \quad \tilde{p}(\chi) = \chi^2 + (d + \mathfrak{b}_1)\chi + d\mathfrak{b}_1 - \frac{\Lambda\beta\eta}{\nu\mu} = 0. \ \square$$

According to Routh's standard [15], the roots of the polynomial $\tilde{p}(\chi)$ have a negative real part if all of its coefficients have the same signal. As a result, the local asymptotic stability of the (DFE) $\mathbf{E}_0$ is established, $\tilde{p}(\chi)$'s coefficients are:

$$\tilde{p}_1 = 1 > 0, \quad \tilde{p}_2 = d + \mathfrak{b}_1 > 0, \quad \tilde{p}_3 = d\mathfrak{b}_1 - \frac{\Lambda\beta\eta}{\nu\mu}.$$

Thus, if

$$d\mathfrak{b}_1 - \frac{\Lambda\beta\eta}{\nu\mu} > 0 \quad \Leftrightarrow \quad \Lambda\beta\eta < (\mu\nu d + \rho\Lambda)(\mu + \delta + \lambda_1).$$

$\mathbf{E}_0$ be locally asymptotically stable.

else if $d\mathfrak{b}_1 - \frac{\Lambda\beta\eta}{\nu\mu} < 0 \quad \Leftrightarrow \quad \Lambda\beta\eta > (\mu\nu d + \rho\Lambda)(\mu + \delta + \lambda_1)$, the DFE is unstable.

else $d\mathfrak{b}_1 = \frac{\Lambda\eta}{\nu\mu} \quad \Leftrightarrow \quad \beta\Lambda\eta = (\mu\nu d + \rho\Lambda)(\mu + \delta + \lambda_1)$, yields a crucial case.

Proposition 2: The equations $\mathfrak{b}_1 = \mu + \delta + \lambda_1$, $\mathfrak{b}_2 = \varepsilon + \mu + \lambda_2$, and $\mathfrak{b}_3 = \mu + \omega$ should be considered. $\delta, \lambda^*, \varepsilon, \omega > 0$ is assumed. Model (16) possesses the equilibrium of endemic if $\mathbf{R}_0 > 1$.

$$\mathbf{E}^* = (\mathcal{Q}^*, \mathcal{I}^*, \mathcal{S}^*, \mathcal{R}^*, \mathcal{B}^*) = \left(\frac{\delta\Lambda\mathfrak{b}_3\lambda^*}{\mathcal{D}}, \frac{\mathfrak{b}_2\Lambda\mathfrak{b}_3\lambda^*}{\mathcal{D}}, \frac{\mathfrak{b}_1\Lambda\mathfrak{b}_2\mathfrak{b}_3}{\mathcal{D}}, \frac{\delta\Lambda\varepsilon\lambda^*}{\mathcal{D}}, \frac{(\eta\beta - \mathfrak{b}_1\rho)\mathfrak{b}_2\Lambda\mathfrak{b}_3\lambda^*}{\mathcal{D}\beta c}\right), \tag{20}$$

where

$$\mathcal{D} = \mathfrak{b}_2\mathfrak{b}_1\mathfrak{b}_3(\mu + \lambda^*) - \varepsilon\delta\omega\lambda^*, \quad \lambda^* = \frac{\mathcal{B}^*\beta}{\mathcal{B}^* + \nu},$$

which is possible if

$$\eta\beta > \mathfrak{b}_1\rho. \tag{21}$$

Proof: The rate of transmission must be entirely positive in order for this equilibrium to be possible:

$$\frac{\beta\mathcal{B}^*(t)}{\mathcal{B}^*(t) + \nu} > 0.$$

The fourth, third and second equilibrium equations of (16) are solved successively, and we discover

$$\mathcal{S}^* = \frac{\mathfrak{b}_1}{\lambda^*}\mathcal{I}^*,$$
$$\mathcal{I}^* = \frac{\mathfrak{b}_2}{\delta}\mathcal{Q}^*,$$
$$\mathcal{Q}^* = \frac{\mathfrak{b}_3}{\varepsilon}\mathcal{R}^*.$$

Next, we get

$$\mathcal{S}^* = \mathcal{R}^*\left(\frac{\mathfrak{b}_2\mathfrak{b}_1\mathfrak{b}_3}{\lambda^*\varepsilon\delta}\right).$$

The final value of $\mathcal{S}^*$ that was assessed is then substituted into the initial equilibrium equation to get

$$\varepsilon\delta\lambda^*\Lambda - \mathcal{R}^*\mathcal{D} = 0.$$

It yields the fourth element of (20) as well as the first three through back substitution. Lastly, the practical value of $\mathcal{B}^*$, which needs to be nonnegative, is given by the fifth equation, which yields (21). Currently, from

$$\lambda^* = \frac{\beta \mathcal{B}^*}{(\nu + \mathcal{B}^*)}.$$

After rearranging and replacing the value of $\mathcal{B}^*$, we get

$$\lambda^* \{[(\beta\eta - \rho b_1)\Lambda + \nu\beta c\mathfrak{b}_1]\mathfrak{b}_3\mathfrak{b}_2 - \beta\nu c\delta\omega\varepsilon\} = [\Lambda\beta\eta - (\nu\mu c)\mathfrak{b}_1 + \Lambda\rho]\,\mathfrak{b}_2\beta\mathfrak{b}_3.$$

Consequently,

$$\lambda^* = \frac{\mathfrak{b}_2\mathfrak{b}_1\mathfrak{b}_3\beta(-1 + \mathbf{R}_0)(\Lambda\rho + c\nu\mu)}{\mathfrak{b}_2\mathfrak{b}_3(\eta\beta - \mathfrak{b}_1\rho)\Lambda + c\beta\nu[\mathfrak{b}_2\mathfrak{b}_1\mathfrak{b}_3 - \varepsilon\delta\omega]}.$$

Considering (21), and the reality that

$$\mathfrak{b}_2\mathfrak{b}_1\mathfrak{b}_3 - \varepsilon\delta\omega = (\lambda_1 + \delta + \mu)(\lambda_2 + \varepsilon + \mu)(\mu + \omega) - \varepsilon\delta\omega > 0.$$

Since all of the other coefficients and $\lambda_1, \lambda_2 \geq 0$ are positive, the value of λ^* above is positive if and only if $\mathbf{R}_0 > 1$. An endemic equilibrium (20) exists in the model (16) in this situation. This brings the proof to an end.

4 The Piecewise Mathematical Model

The piecewise cholera mathematical model presented in this study enhances conventional epidemic modeling by employing sophisticated, multi-stage fractional differential equations to accurately capture the dynamics of cholera transmission. The model divides the progression of the disease into four distinct periods, each representing a critical stage in the spread of the infection. To reflect the unique characteristics of disease propagation at each stage, a different fractional derivative operator is applied within each interval.

In the initial phase $0 < t \leq T_1$, the model (16) utilizes the Caputo-Fabrizio fractional derivative, which provides a smooth representation of early-stage dynamics. This derivative effectively characterizes the rapid initial spread of the disease, with minimal memory effects influencing transmission.

During the second phase $T_1 < t \leq T_2$, the model (16) incorporates a proportional constant hybrid Caputo operator. This stage reflects the cumulative impact of infection, accounting for evolving interactions and immune responses as the disease progresses.

In the advanced stages of cholera, when $T_2 < t \leq T_3$, the model described in system (16) incorporates the Atangana-Baleanu fractional derivative. This operator is particularly effective in capturing the complex and irregular transmission patterns that emerge in the later stages of an outbreak. As the disease progresses, its spread becomes more unpredictable, making the Atangana-Baleanu derivative a suitable choice for modeling these dynamics.

The stochastic cholera model for $T_3 < t \leq T_f$ offers a more realistic representation of disease transmission by incorporating environmental and epidemiological randomness. Unlike deterministic models, it accounts for unpredictable fluctuations in disease dynamics, leading to improved epidemic forecasting and more effective strategies for adaptive public health interventions.

By adopting this piecewise differential approach, the model offers a more realistic and comprehensive depiction of epidemic stages, significantly improving predictive insights into the progression and potential containment of cholera outbreaks.

The resulting system is expressed as follows:

$$\begin{cases} \frac{1}{\vartheta^{1-\alpha}} {}^{CF}_{0}D^{\alpha}_{\mathfrak{t}}\mathcal{S}(\mathfrak{t}) = -\frac{\beta\mathcal{B}(\mathfrak{t})\mathcal{S}(\mathfrak{t})}{\nu+\mathcal{B}(\mathfrak{t})} + \omega\mathcal{R}(\mathfrak{t}) - \mu\mathcal{S}(\mathfrak{t}) + \nabla, \\ \frac{1}{\vartheta^{1-\alpha}} {}^{CF}_{0}D^{\alpha}_{\mathfrak{t}}\mathcal{I}(\mathfrak{t}) = \frac{\beta\mathbb{B}(\mathfrak{t})\mathcal{S}(\mathfrak{t})}{\nu+\mathcal{B}(\mathfrak{t})} - (\delta+\lambda_1+\mu)\mathcal{I}(\mathfrak{t}), \\ \frac{1}{\vartheta^{1-\alpha}} {}^{CF}_{0}D^{\alpha}_{\mathfrak{t}}\mathcal{Q}(\mathfrak{t}) = -(\lambda_2+\varepsilon+\mu)\mathcal{Q}(\mathfrak{t}) + \delta\mathcal{I}(\mathfrak{t}), \quad 0 < \mathfrak{t} \le T_1, \\ \frac{1}{\vartheta^{1-\alpha}} {}^{CF}_{0}D^{\alpha}_{\mathfrak{t}}\mathcal{R}(\mathfrak{t}) = -(\mu+\omega)\mathcal{R}(\mathfrak{t}) + \varepsilon\mathcal{Q}(\mathfrak{t}), \\ \frac{1}{\vartheta^{1-\alpha}} {}^{CF}_{0}D^{\alpha}_{\mathfrak{t}}\mathcal{B}(\mathfrak{t}) = -d\mathcal{B}(\mathfrak{t}) - \frac{\rho\mathcal{B}(\mathfrak{t})\mathcal{S}(\mathfrak{t})}{\nu+\mathcal{B}(\mathfrak{t})} + \eta\mathcal{I}(\mathfrak{t}), \end{cases} \tag{22}$$

with initial conditions

$$\mathcal{Q}_0 \ge 0,\ \mathcal{I}_0 \ge 0, \mathcal{S}_0 \ge 0, \mathcal{R}_0 \ge 0, \mathcal{B}_0 \ge 0. \tag{23}$$

$$\begin{cases} \frac{1}{\vartheta^{1-\alpha}} {}^{CPC}_{0}D^{\alpha}_{\mathfrak{t}}\mathcal{S}(\mathfrak{t}) = -\frac{\beta\mathcal{B}(\mathfrak{t})\mathcal{S}(\mathfrak{t})}{\nu+\mathcal{B}(\mathfrak{t})} + \omega\mathcal{R}(\mathfrak{t}) - \mu\mathcal{S}(\mathfrak{t}) + \nabla, \\ \frac{1}{\vartheta^{1-\alpha}} {}^{CPC}_{0}D^{\alpha}_{\mathfrak{t}}\mathcal{I}(\mathfrak{t}) = \frac{\beta\mathcal{B}(\mathfrak{t})\mathcal{S}(\mathfrak{t})}{\nu+\mathcal{B}(\mathfrak{t})} - (\delta+\lambda_1+\mu)\mathcal{I}(\mathfrak{t}), \\ \frac{1}{\vartheta^{1-\alpha}} {}^{CPC}_{0}D^{\alpha}_{\mathfrak{t}}\mathcal{Q}(\mathfrak{t}) = -(\lambda_2+\varepsilon+\mu)\mathcal{Q}(\mathfrak{t}) + \delta\mathcal{I}(\mathfrak{t}), T_1 < \mathfrak{t} \le T_2, \\ \frac{1}{\vartheta^{1-\alpha}} {}^{CPC}_{0}D^{\alpha}_{\mathfrak{t}}\mathcal{R}(\mathfrak{t}) = -(\mu+\omega)\mathcal{R}(\mathfrak{t}) + \varepsilon\mathcal{Q}(\mathfrak{t}), \\ \frac{1}{\vartheta^{1-\alpha}} {}^{CPC}_{0}D^{\alpha}_{\mathfrak{t}}\mathcal{B}(\mathfrak{t}) = -d\mathcal{B}(\mathfrak{t}) - \frac{\rho\mathcal{B}(\mathfrak{t})\mathcal{S}(\mathfrak{t})}{\nu+\mathcal{B}(\mathfrak{t})} + \eta\mathcal{I}(\mathfrak{t}), \end{cases} \tag{24}$$

with initial conditions

$$\mathcal{Q}(\mathfrak{t}_1) \ge 0,\ \mathcal{I}(\mathfrak{t}_1) \ge 0, \mathcal{S}(\mathfrak{t}_1) \ge 0, \mathcal{R}(\mathfrak{t}_1) \ge 0, \mathcal{B}(\mathfrak{t}_1) \ge 0. \tag{25}$$

$$\begin{cases} \frac{1}{\vartheta^{1-\alpha}} {}^{ABC}_{0}D^{\alpha}_{\mathfrak{t}}\mathcal{S}(\mathfrak{t}) = -\frac{\beta\mathcal{B}(\mathfrak{t})\mathcal{S}(\mathfrak{t})}{\nu+\mathcal{B}(\mathfrak{t})} + \omega\mathcal{R}(\mathfrak{t}) - \mu\mathcal{S}(\mathfrak{t}) + \nabla, \\ \frac{1}{\vartheta^{1-\alpha}} {}^{ABC}_{0}D^{\alpha}_{\mathfrak{t}}\mathcal{I}(\mathfrak{t}) = \frac{\beta\mathcal{B}(\mathfrak{t})\mathcal{S}(\mathfrak{t})}{\nu+\mathcal{B}(\mathfrak{t})} - (\delta+\lambda_1+\mu)\mathcal{I}(\mathfrak{t}), \\ \frac{1}{\vartheta^{1-\alpha}} {}^{ABC}_{0}D^{\alpha}_{\mathfrak{t}}\mathcal{Q}(\mathfrak{t}) = -(\lambda_2+\varepsilon+\mu)\mathcal{Q}(\mathfrak{t}) + \delta\mathcal{I}(\mathfrak{t}), \quad T_2 < \mathfrak{t} \le T_3, \\ \frac{1}{\vartheta^{1-\alpha}} {}^{ABC}_{0}D^{\alpha}_{\mathfrak{t}}\mathcal{R}(\mathfrak{t}) = -(\mu+\omega)\mathcal{R}(\mathfrak{t}) + \varepsilon\mathcal{Q}(\mathfrak{t}), \\ \frac{1}{\vartheta^{1-\alpha}} {}^{ABC}_{0}D^{\alpha}_{\mathfrak{t}}\mathcal{B}(\mathfrak{t}) = -d\mathcal{B}(\mathfrak{t}) - \frac{\rho\mathcal{B}(\mathfrak{t})\mathcal{S}(\mathfrak{t})}{\nu+\mathcal{B}(\mathfrak{t})} + \eta\mathcal{I}(\mathfrak{t}), \end{cases} \tag{26}$$

with

$$\mathcal{Q}(\mathfrak{t}_2) = \mathcal{S}_2 \ge 0,\ \mathcal{I}(\mathfrak{t}_2) = \mathcal{I}_2 \ge 0, \mathcal{S}(\mathfrak{t}_2) = \mathcal{Q}_2 \ge 0, \mathcal{R}(\mathfrak{t}_2) = \mathcal{R}_2 \ge 0,$$
$$\mathcal{B}(\mathfrak{t}_2) = \mathcal{B}_2 \ge 0. \tag{27}$$

$$\begin{cases} d\mathcal{S}(\mathrm{t}) = \left(-\dfrac{\beta\mathcal{B}(\mathrm{t})\mathcal{S}(\mathrm{t})}{\nu+\mathbb{B}(\mathrm{t})} + \omega\mathbb{R}(\mathrm{t}) - \mu\mathcal{S}(\mathrm{t}) + \nabla\right)dt + \sigma_1\mathcal{S}(\mathrm{t})dW_1, \\ d\mathrm{t}\mathcal{I}(\mathrm{t}) = \left(\dfrac{\beta\mathcal{B}(\mathrm{t})\mathcal{S}(\mathrm{t})}{\nu+\mathcal{B}(\mathrm{t})} - (\delta+\lambda_1+\mu)\mathcal{I}(\mathrm{t})\right)dt + \sigma_2\mathcal{I}(\mathrm{t})dW_2, \\ d\mathcal{Q}(\mathrm{t}) = (-(\lambda_2+\varepsilon+\mu)\mathcal{Q}(\mathrm{t}) + \delta\mathcal{I}(\mathrm{t}))\,dt + \sigma_3\mathcal{Q}(\mathrm{t})dW_3, \quad T_3 < \mathrm{t} \le T_f, \\ d\mathcal{R}(\mathrm{t}) = (-(\omega+\mu)\mathcal{R}(\mathrm{t}) + \varepsilon\mathcal{Q}(\mathrm{t}))\,dt + \sigma_4\mathcal{R}(\mathrm{t})dW_4, \\ d\mathcal{B}(\mathrm{t}) = \left(-d\mathcal{B}(\mathrm{t}) - \dfrac{\rho\mathcal{B}(\mathrm{t})\mathcal{S}(\mathrm{t})}{\nu+\mathcal{B}(\mathrm{t})} + \eta\mathcal{I}(\mathrm{t})\right)dt + \sigma_5\mathcal{B}(\mathrm{t})dW_5, \end{cases} \tag{28}$$

where $\sigma_i, \quad i = 1, 2, \ldots, 5$, represents the real constants of the stochastic environment intensity, and dW_i describes the standard Brownian motion. with

$$\mathcal{Q}(\mathrm{t}_3) = \mathcal{S}_3 \ge 0,\ \mathcal{I}(\mathrm{t}_3) = \mathcal{I}_3 \ge 0, \mathcal{S}(\mathrm{t}_3) = \mathcal{Q}_3 \ge 0, \mathcal{R}(\mathrm{t}_3) = \mathcal{R}_3 \ge 0, \quad \mathcal{B}(\mathrm{t}_3) = \mathcal{B}_3 \ge 0. \tag{29}$$

5 Numerical Approach to Solving the Proposed Model

5.1 Numerical Scheme with Exponential Decay Kernel

Consider the hybrid fractional order derivatives equation that follows:

$$\begin{aligned} &{}_0^{CF}D_{\mathrm{t}}^{\alpha}\mathcal{Z}(\mathrm{t}) = \mathcal{P}(\mathrm{t}, \mathcal{Z}(\mathrm{t})), \quad 0 < \alpha \le 1, \\ &\mathcal{Z}(0) = \mathcal{Z}_0. \end{aligned}$$

Rewriting the above equation as [11] is possible based on Caputo-Fabrizio's definition integral (8):

$$\mathcal{Z}(\mathrm{t}) - \mathcal{Z}(0) = \frac{-\alpha+1}{\mathcal{N}(\alpha)}\mathcal{P}(\mathrm{t}, \mathcal{Z}(\mathrm{t})) + \frac{\alpha}{\mathcal{N}(\alpha)}\int_0^{\mathrm{t}} \mathcal{P}(\tau, \mathcal{Z}(\kappa))\,d\kappa, \tag{30}$$

We write (30) at $\mathrm{t}_{1+k} = (1+k)\Delta\mathrm{t}$,

$$\mathcal{Z}(\mathrm{t}_{1+k}) - \mathcal{Z}(0) = \frac{-\alpha+1}{\mathcal{N}(\alpha)}\mathcal{P}(\mathrm{t}_k, \mathcal{Z}(\mathrm{t}_k)) + \frac{\alpha}{\mathcal{N}(\alpha)}\int_0^{\mathrm{t}_{1+k}} \mathcal{P}(t_\kappa, \mathcal{Z}(t_\kappa))\,d\kappa,$$

and at $\mathrm{t}_k = k\Delta\mathrm{t}$:

$$\mathcal{Z}(\mathrm{t}_k) - \mathcal{Z}(0) = \frac{-\alpha+1}{\mathcal{N}(\alpha)}\mathcal{P}(\mathrm{t}_{-1+k}, \mathcal{Z}(\mathrm{t}_{-1+k})) + \frac{\alpha}{\mathcal{N}(\alpha)}\int_0^{\mathrm{t}_k} \mathcal{P}(t_\kappa, \mathcal{Z}(t_\kappa))\,d\kappa,$$

where the normalization function $\mathcal{N}(\alpha)$ ensures that $\mathcal{N}(0) = 1$ and $\mathcal{N}(1) = 1$.

Using these equations' various approaches, the following can be written [11]:

$$\begin{aligned} \mathcal{Z}(\mathrm{t}_{1+k}) - \mathcal{Z}(\mathrm{t}_k) = {} & \frac{-\alpha+1}{\mathcal{N}(\alpha)}\left[\mathcal{P}(\mathrm{t}_k, \mathcal{Z}(\mathrm{t}_k)) - \mathcal{P}(\mathrm{t}_{-1+k}, \mathcal{Z}(\mathrm{t}_{-1+k}))\right] \\ & + \frac{\alpha}{\mathcal{N}(\alpha)}\int_{\mathrm{t}_k}^{\mathrm{t}_{1+k}} \mathcal{P}(t_\kappa, \mathcal{Z}(t_\kappa))\,d\kappa. \end{aligned}$$

The following can be obtained by entering its Lagrange polynomial into the equation above:

$$\mathcal{Z}^{1+k} - \mathcal{Z}^k = \frac{-\alpha+1}{\mathcal{N}(\alpha)}\left[\mathcal{P}(\mathrm{t}_k, \mathcal{Z}(\mathrm{t}_k)) - \mathcal{P}(\mathrm{t}_{-1+k}, \mathcal{Z}(\mathrm{t}_{-1+k}))\right]$$

$$+\frac{\alpha}{\mathcal{N}(\alpha)}\int_{t_k}^{t_{1+k}}\left[\frac{\mathcal{P}(t_k,\mathcal{Z}(t_k))}{\Delta t}(\kappa-t_{-1+k})-\frac{\mathcal{P}(t_{-1+k},\mathcal{Z}(t_{-1+k}))}{\Delta t}(\kappa-t_k)\right]d\kappa,$$

and we get the following:

$$\begin{aligned}\mathcal{Z}^{1+k}-\mathcal{Z}^k&=\frac{-\alpha+1}{\mathcal{N}(\alpha)}\left[\mathcal{P}(t_k,\mathcal{Z}(t_k))-\mathcal{P}(t_{-1+k},Z(t_{-1+k}))\right]\\&+\frac{\alpha}{\mathcal{N}(\alpha)}\left[\frac{\mathcal{P}(t_k,\mathcal{Z}(t_k))}{\Delta t}\int_{t_k}^{t_{1+k}}(\kappa-t_{-1+k})\,d\kappa\right.\\&\left.-\frac{\mathcal{P}(t_{-1+k},\mathcal{Z}(t_{-1+k}))}{\Delta t}\int_{t_k}^{t_{1+k}}(\kappa-t_k)\,d\kappa\right].\end{aligned}$$

Calculating the integrals on the equation above's right side is possible as:

$$\int_{t_k}^{t_{1+k}}(-t_{-1+k}+\kappa)\,d\kappa=\frac{3}{2}(\Delta t)^2,$$
$$\int_{t_k}^{t_{1+k}}(-t_k+\kappa)\,d\kappa=\frac{1}{2}(\Delta t)^2.$$

Consequently, the following numerical scheme is:

$$\begin{aligned}\mathcal{Z}^{1+k}&=\mathcal{Z}^k+\frac{-\alpha+1}{\mathcal{N}(\alpha)}\left[\mathcal{P}(t_k,\mathcal{Z}(t_k))-\mathcal{P}(t_{-1+k},\mathcal{Z}(t_{-1+k}))\right]\\&+\frac{\alpha}{\mathcal{N}(\alpha)}\left[\mathcal{P}(t_k,\mathcal{Z}^k)\cdot\frac{3}{2}\Delta t-\mathcal{P}(t_{-1+k},\mathcal{Z}^{(-1+k)})\cdot\frac{1}{2}\Delta t\right].\end{aligned}\tag{31}$$

Stability of Numerical Scheme with Exponential Decay Kernel

We employ spectral stability analysis to examine the stability of the specified numerical system. We presume that the function $\mathcal{P}(t,\mathcal{Z}(t))$ in this instance is linear, so it can be represented as $\mathcal{P}(t,\mathcal{Z}(t))=\lambda\mathcal{Z}$, where λ is a constant that reflects the effect of $\mathcal{P}$ on the solution $\mathcal{Z}$.

With this approximation, we can rewrite the numerical Eq. (31) as follows [11]:

$$\begin{aligned}\mathcal{Z}_{k+1}&=\mathcal{Z}_k+\frac{1-\alpha}{\mathcal{N}(\alpha)}\cdot(\lambda\mathcal{Z}_k-\lambda\mathcal{Z}_{k-1})\\&+\frac{\alpha}{\mathcal{N}(\alpha)}\left(\lambda\mathcal{Z}_k\cdot\frac{3}{2}\Delta t-\lambda\mathcal{Z}_{k-1}\cdot\frac{1}{2}\Delta t\right).\end{aligned}$$

After simplifying, the recurrence relation becomes:

$$\begin{aligned}\mathcal{Z}_{1+k}&=\mathcal{Z}_k\left(1+\frac{\lambda\Delta t}{\mathcal{N}(\alpha)}\left((1-\alpha)+\frac{3}{2}\alpha\right)\right)\\&-\mathcal{Z}_{-1+k}\left(\frac{\Delta t*\lambda}{\mathcal{N}(\alpha)}\left((1-\alpha)+\frac{1}{2}\alpha\right)\right).\end{aligned}$$

To achieve stability, the absolute values of the numerical coefficients in the recurrence relation must be less than or equal to 1. The main stability condition is:

$$\left|1+\frac{\lambda\Delta t}{\mathcal{N}(\alpha)}\left((1-\alpha)+\left(\frac{3}{2}\right)\alpha\right)\right|\le 1.$$

By rearranging the inequality as follows, we may obtain an upper bound for Δt from this condition:

$$\Delta t \leq \frac{2\mathcal{N}(\alpha)}{\lambda\left((1-\alpha)+\left(\frac{3}{2}\right)\alpha\right)}.$$

Thus, stability is ensured if we select a time step Δt that is less than or equal to this bound, which depends on the values of λ, $\mathcal{N}(\alpha)$, and α.

5.2 CPC-GLNFDM

Consider the hybrid fractional order derivatives equation that follows:

$$\left({}_0^{CPC}D_t^{\alpha}\mathcal{Z}\right)(t) = \mathcal{Z}(t), \quad 0 < \alpha \leq 1, \quad \mathcal{Z}(0) = \mathcal{Z}_0. \tag{32}$$

The following is an expression for the relationship (10) [10]:

$$\begin{aligned} {}_0^{CPC}D_t^{\alpha}\mathcal{Z}(t) &= \frac{1}{\Gamma(1-\alpha)}\int_0^t (-\mathfrak{s}+t)^{-\alpha}(\mathcal{G}_1(\alpha)\mathcal{Z}(\mathfrak{s}) + \mathcal{G}_0(\alpha)\mathcal{Z}'(\mathfrak{s}))d\mathfrak{s}, \\ &= \mathcal{G}_1(\alpha){}_0^{RL}I_t^{1-\alpha}\mathcal{Z}(t) + \mathcal{G}_0(\alpha){}_0^{C}D_t^{\alpha}\mathcal{Z}(t), \\ &= \mathcal{G}_1(\alpha){}_0^{RL}D_t^{\alpha-1}\mathcal{Z}(t) + \mathcal{G}_0(\alpha){}_0^{C}D_t^{\alpha}\mathcal{Z}(t). \end{aligned} \tag{33}$$

In this case, $\mathcal{G}_1(\alpha)$ and $\mathcal{G}_0(\alpha)$ rely solely on α. The following is how we can use CPC-GLNFDM to approximate (33):

$$\begin{aligned} {}_0^{CPC}D_t^{\alpha}\mathcal{Z}(t)|_{t=t^n} &= \frac{\mathcal{G}_1(\alpha)}{(\Theta(\Delta t))^{\alpha-1}}\left(\mathcal{Z}_{1+n} + \sum_{i=1}^{1+n} u_i\mathcal{Z}_{1+n-i}\right) \\ &\quad + \frac{\mathcal{G}_0(\alpha)}{(\Theta(\Delta t))^{\alpha}}\left(\mathcal{Z}_{1+n} - \sum_{i=1}^{1+n}\mu_i\mathcal{Z}_{1+n-i} - \mathfrak{q}_{1+n}\mathcal{Z}_0\right), \end{aligned}$$

$$\begin{aligned} &\frac{\mathcal{G}_1(\alpha)}{(\Theta(\Delta t))^{-1+\alpha}}\left(\mathcal{Z}_{1+n} + \sum_{i=1}^{1+n} u_i\mathcal{Z}_{1+n-i}\right) + \frac{\mathcal{G}_0(\alpha)}{(\Theta(\Delta t))^{\alpha}}\left(\mathcal{Z}_{1+n} - \sum_{i=1}^{1+n}\mu_i\mathcal{Z}_{1+n-i} - \mathfrak{q}_{1+n}\mathcal{Z}_0\right) \\ &= \mathcal{Z}(t_n), \end{aligned} \tag{34}$$

and $\Theta(\Delta t) = \Delta t + O(\Delta t^2)$, $0 < \Theta(\Delta t) < 1$, $\Delta t \longrightarrow 0$. $u_0 = 1$, $u_i = (1-\frac{\alpha}{i})u_{i-1}$, $t^n = n(\Theta(\Delta t))$, $\Delta t = \frac{T_f}{N_n}$, $\mathcal{N}_n$ is a number which is natural.

$\mu_i = (-1)^{-1+i}\binom{\alpha}{i}$, $\mu_1 = \alpha$, $\mathfrak{q}_i = \frac{i^{\alpha}}{\Gamma(-\alpha+1)}$ and $i = 1, 2, \ldots, n+1$. Also, let us assume that [16]

$$0 < \mu_{1+i} < \mu_i < \ldots < \mu_1 = \alpha(t) < 1,$$
$$0 < \mathfrak{q}_{i+1} < \mathfrak{q}_i < \ldots < \mathfrak{q}_1 = \frac{1}{\Gamma(-\alpha+1)}.$$

Remark 1. *If $\mathcal{G}_1(\alpha) = 0$ and $\mathcal{G}_0(\alpha) = 1$ in (34), we have the approximation of Caputo fractional derivative with Grünwald-Letnikov nonstandard finite difference method (C-GLFDM).*

Stability of CPC-GLNFDM

Consider a model test problem of linear fractional order delay differential equation [17] to examine the stability of the suggested approach (34).

Assuming that $\mathcal{Z}(\mathfrak{t}_{\mathfrak{n}}) = \mathcal{Z}_{\mathfrak{n}}$ is the closest solution to this equation, by the application of CPC-NFDM in conjunction with relation (10) allows us to reformulate Eq. (33) as follows:

$$\frac{\mathcal{G}_1(\alpha)}{\Theta(\Delta\mathfrak{t})^{-1+\alpha}}\left(\mathcal{Z}_{1+\mathfrak{n}} + \sum_{i=1}^{1+\mathfrak{n}} u_i \mathcal{Z}_{1+\mathfrak{n}-i}\right) + \frac{\mathcal{G}_0(\alpha)}{\Theta(\Delta\mathfrak{t})^{\alpha}}\left(\mathcal{Z}_{\mathfrak{n}+1} - \sum_{i=1}^{1+\mathfrak{n}} \mu_i \mathcal{Z}_{\mathfrak{n}+1`-i} - \mathfrak{q}_{\mathfrak{n}+1}\mathcal{Z}_0\right)$$
$$= (\rho_0 \mathcal{Z}(\mathfrak{t}_{\mathfrak{n}})),$$

we put

$$gg = \frac{\mathcal{G}_1(\alpha)}{\Theta(\Delta\mathfrak{t})^{\alpha-1}}$$

and

$$gg1 = \frac{\mathcal{G}_0(\alpha)}{\Theta(\Delta\mathfrak{t})^{\alpha}},$$

we get

$$\mathcal{Z}_{1+\mathfrak{n}} = \frac{1}{(gg + gg1)}\left(gg1 \sum_{i=1}^{1+\mathfrak{n}} \mu_i \mathcal{Z}_{1+\mathfrak{n}-i} - \mathfrak{q}_{1+\mathfrak{n}}\mathcal{Z}_0 - gg \sum_{i=1}^{1+\mathfrak{n}} \omega_i \mathcal{Z}_{1+\mathfrak{n}-i} - (\mathcal{Z}(t_{\mathfrak{n}}))\right),$$

we have

$$\frac{1}{(gg + gg1)} < 1,$$
$$\mathcal{Z}_1 \leq \mathcal{Z}_0,$$
$$\mathcal{Z}_{\mathfrak{n}} \leq \mathcal{Z}_{\mathfrak{n}-1} \leq \mathcal{Z}_{\mathfrak{n}-2} \leq \ldots \leq \mathcal{Z}_1 \leq \mathcal{Z}_0.$$

Accordingly, the suggested scheme is stable.

5.3 Toufik-Atangana method

Let's look at the Mittag-Leffler kernel Cauchy problem:

$$\prescript{ABC}{0}{D}_{\mathfrak{t}}^{\alpha}\mathcal{Z}(\mathfrak{t}) = \mathcal{P}(\mathfrak{t}, \mathcal{Z}(\mathfrak{t})), \quad 0 < \alpha \leq 1, \tag{35}$$

$$\mathcal{Z}(0) = \mathcal{Z}_0,$$

we transform (35) into

$$\mathcal{Z}(\mathfrak{t}) - \mathcal{Z}(0) = \frac{1-\alpha}{\mathcal{AB}(\alpha)}\mathcal{Z}(\mathfrak{t}) + \frac{\alpha}{\mathcal{AB}(\alpha)\Gamma(\alpha)}\int_0^{\mathfrak{t}} \mathcal{P}(\kappa, \mathcal{Z}(\kappa))(-\kappa + \mathfrak{t})^{-1+\alpha} d\kappa.$$

At the temporal point $\mathfrak{t}_{1+k} = (1+k)\Delta\mathfrak{t}$, the following is founded:

$$\mathcal{Z}(\mathfrak{t}_{1+k}) - \mathcal{Z}(0) = \frac{-\alpha+1}{\mathcal{AB}(\alpha)}\mathcal{P}(\mathfrak{t}, \mathcal{Z}(\mathfrak{t}))$$

$$+\frac{\alpha}{\mathcal{AB}(\alpha)}\int_0^{t_{1+k}}\mathcal{P}(\kappa,\mathcal{Z}(\kappa))(-\kappa+t_{1+k})^{-1+\alpha}\,d\kappa,$$

and we write

$$\mathcal{Z}(t_{1+k})=\mathcal{Z}(0)+\frac{-\alpha+1}{\mathcal{AB}(\alpha)}\mathcal{P}(t_k,\mathcal{Z}^k)+\frac{\alpha}{\mathcal{AB}(\alpha)\Gamma(\alpha)}\sum_{\mathfrak{h}=0}^{k}\int_{t_\mathfrak{h}}^{t_{1+\mathfrak{h}}}\mathcal{P}(\kappa,\mathcal{Z}(\kappa))(t_{1+k}-\kappa)^{-1+\alpha}\,d\kappa. \tag{36}$$

The above equation can be expressed as follows once its Lagrange polynomial has been entered into (36) as an approximation of the function's behavior $\mathcal{P}(\kappa,\mathcal{Z}(\kappa))$:

$$\mathcal{Z}_{(1+k)}=\mathcal{Z}_0+\frac{1-\alpha}{\mathcal{AB}(\alpha)}[\mathcal{P}(t_k,\mathcal{Z}_k)]+\frac{\alpha}{\mathcal{AB}(\alpha)\Gamma(\alpha)}\sum_{\mathfrak{h}=0}^{k}\int_{t_\mathfrak{h}}^{t_{1+\mathfrak{h}}}\Big[\frac{\mathcal{P}(t_\mathfrak{h},\mathcal{Z}_\mathfrak{h})}{\Delta t}(\kappa-t_{t-1})-\frac{\mathcal{P}(t_{\mathfrak{h}-1},\mathcal{Z}_{\mathfrak{h}-1}))}{\Delta t}(\kappa-t_\mathfrak{h})\Big](t_{k+1}-\kappa)^{\alpha-1}d\kappa.$$

Thus, we get

$$\mathcal{Z}_{k+1}=\mathcal{Z}_0+\frac{1-\alpha}{\mathcal{AB}(\alpha)}[\mathcal{P}(t_k,\mathcal{Z}_k)]+\frac{\alpha}{\mathcal{AB}(\alpha)\Gamma(\alpha)}\sum_{\mathfrak{h}=0}^{k}\left[\int_{t_\mathfrak{h}}^{t_{1+\mathfrak{h}}}\frac{\mathcal{P}(t_\mathfrak{h},\mathcal{Z}_\mathfrak{h})}{\Delta t}(\kappa-t_{\mathfrak{h}-1})(t_{k+1}-\kappa)^{\alpha-1}\,d\kappa-\int_{t_\mathfrak{h}}^{t_{1+\mathfrak{h}}}\frac{\mathcal{P}(t_{\mathfrak{h}-1},\mathcal{Z}_{\mathfrak{h}-1})}{\Delta t}(\tau-t_\mathfrak{h})(t_{k+1}-\kappa)^{\alpha-1}\,d\kappa\right],$$

and

$$\mathcal{Z}_{k+1}=\mathcal{Z}_0+\frac{1-\alpha}{\mathcal{AB}(\alpha)}[\mathcal{P}(t_k,\mathcal{Z}_k)]+\frac{\alpha}{\mathcal{AB}(\alpha)\Gamma(\alpha)}\sum_{\mathfrak{h}=0}^{k}\frac{\mathcal{P}(t_\mathfrak{h},\mathcal{Z}_\mathfrak{h})}{\Delta t}\int_{t_\mathfrak{h}}^{t_{\mathfrak{h}+1}}(\kappa-t_{\mathfrak{h}-1})(t_{k+1}-\kappa)^{\alpha-1}\,d\kappa-\frac{\alpha}{\mathcal{AB}(\alpha)\Gamma(\alpha)}\sum_{\mathfrak{h}=0}^{k}\frac{\mathcal{P}(t_{\mathfrak{h}-1},\mathcal{Z}_{\mathfrak{h}-1})}{\Delta t}\int_{t_\mathfrak{h}}^{t_{\mathfrak{h}+1}}(\kappa-t_\mathfrak{h})(t_{k+1}-\kappa)^{\alpha-1}\,d\kappa. \tag{37}$$

we can calculate the above integrals in (37) as follows:

$$\int_{t_\mathfrak{h}}^{t_{\mathfrak{h}+1}}(\kappa-t_{\mathfrak{h}-1})(t_{k+1}-\kappa)^{\alpha-1}\,d\kappa=\frac{(\Delta t)^{\alpha+1}}{\alpha(\alpha+1)}\Big[(k+1-\mathfrak{h})^{\alpha}(k+2+\alpha-\mathfrak{h})-(k-\mathfrak{h})^{\alpha}(k+2+2\alpha-\mathfrak{h})\Big],$$

$$\int_{t_\mathfrak{h}}^{t_{\mathfrak{h}+1}}(\kappa-t_\mathfrak{h})(t_{k+1}-\kappa)^{\alpha-1}\,d\kappa=\frac{(\Delta t)^{\alpha+1}}{\alpha(\alpha+1)}\Big[(k+1-\mathfrak{h})^{\alpha+1}-(k-\mathfrak{h})^{\alpha}(k+1+\alpha-\mathfrak{h})\Big].$$

After entering these computations into (37), we obtain the numerical approximation [11]:

$$\begin{aligned}\mathcal{Z}_{k+1} &= \mathcal{Z}_0 + \frac{(1-\alpha)}{\mathcal{AB}(\alpha)}\left[\mathcal{P}(\mathfrak{t}_k, \mathcal{Z}_k)\right] \\ &+ \frac{\alpha(\Delta \mathfrak{t})^\alpha}{\mathcal{AB}(\alpha)\Gamma(\alpha+2)}\sum_{\mathfrak{h}=0}^{k}\mathcal{P}(\mathfrak{t}_\mathfrak{h}, \mathcal{Z}_\mathfrak{h})\Big[(k+1-\mathfrak{h})^\alpha(k+2+\alpha-\mathfrak{h}) \\ &- (k-\mathfrak{h})^\alpha(k+2+2\alpha-\mathfrak{h})\Big] \\ &- \frac{\alpha(\Delta t)^\alpha}{\mathcal{AB}(\alpha)\Gamma(\alpha+2)}\sum_{\mathfrak{h}=0}^{k}\mathcal{P}(\mathfrak{t}_{\mathfrak{h}-1}, \mathcal{Z}_{\mathfrak{h}-1})\Big[(k+1-\mathfrak{h})^{\alpha+1} - (k-\mathfrak{h})^\alpha(k+1+\alpha-\mathfrak{h})\Big]. \end{aligned} \tag{38}$$

Stability of Toufik-Atangana Method

The stability of the Atangana-Baleanu method is examined by analyzing the errors arising from the numerical solution of the given Cauchy problem. Let's begin with the general form of the Atangana-Baleanu fractional derivative in the Caputo sense, represented by [11]:

$${}_0^{ABC}D_\mathfrak{t}^\alpha \mathcal{Z}(\mathfrak{t}) = \frac{\mathcal{AB}(\alpha)}{-\alpha+1}\int_a^\mathfrak{t}\dot{\mathcal{Z}}(\kappa)E_\alpha\left[-\frac{\alpha}{-\alpha+1}(-\kappa+\mathfrak{t})^\alpha\right]d\kappa.$$

Applying this method to the equation

$$\begin{aligned}\mathcal{Z}(\mathfrak{t}) - \mathcal{Z}(0) &= \frac{-\alpha+1}{\mathcal{AB}(\alpha)}\mathcal{Z}(\mathfrak{t}) \\ &+ \frac{\alpha}{\mathcal{AB}(\alpha)\Gamma(\alpha)}\int_0^\mathfrak{t}\mathcal{P}(\kappa, \mathcal{Z}(\kappa))(-\kappa+\mathfrak{t})^{-1+\alpha}d\kappa.\end{aligned}$$

We proceed to obtain a stability criterion. Let $\mathcal{Z}_k$ represent the numerical solution at the time point $\mathfrak{t}_k$. Assuming the approximate solution can be expressed as:

$$\mathcal{Z}_k = \mathcal{Z}^* + e_k,$$

where $\mathcal{Z}^*$ is the exact solution and e_k denotes the error at point k. The following expression represents the error:

$$\begin{aligned}\mathcal{Z}_{k+1} - \mathcal{Z}(0) &= \frac{1-\alpha}{\mathcal{AB}(\alpha)}\mathcal{P}(\mathfrak{t}_k, \mathcal{Z}_k) \\ &+ \frac{\alpha}{\mathcal{AB}(\alpha)\Gamma(\alpha)}\sum_{\mathfrak{h}=0}^{k}\int_{t_\mathfrak{h}}^{\mathfrak{t}_{1+\mathfrak{h}}}\mathcal{P}(\kappa, \mathcal{Z}(\kappa))(\mathfrak{t}_{k+1}-\kappa)^{-1+\alpha}d\kappa.\end{aligned}$$

For the numerical scheme given in Eq. (38) to remain stable, the time step Δt must be chosen appropriately. Based on the fractional-order formulation and stability analysis, we impose the condition:

$$\Delta t \leq \frac{2AB(\alpha)\Gamma(\alpha+2)}{\alpha \max|P(t,Z)|}.$$

This ensures that numerical errors remain controlled, preventing divergence in long-term simulations and ensuring stability by controlling the growth of numerical errors.

5.4 Numerical Methods for Solving the Crossover Model

We provide numerical methods for solving (22)–(29) in this section. Our method for addressing the ensuing linear crossover model is given as follows:

$$ {}_{0}^{CF}D_{\mathfrak{t}}^{\alpha}\mathcal{Z} = \Lambda(\mathcal{Z},\mathfrak{t}), \quad 1 \geq \alpha > 0, \quad 0 < \mathfrak{t} \leq T_1, \tag{39}$$

$$\mathcal{Z}(\mathfrak{t}_0) = \mathcal{Z}_0,$$

$$ {}_{0}^{CPC}D_{\mathfrak{t}}^{\alpha}\mathcal{Z} = \Lambda(\mathcal{Z},\mathfrak{t}), \quad 1 \geq \alpha > 0, \quad T_1 < \mathfrak{t} \leq T_2, \tag{40}$$

$$\mathcal{Z}(\mathfrak{t}_1) = \mathcal{Z}_l,$$

$$ {}_{0}^{ABC}D_{\mathfrak{t}}^{\alpha}\mathcal{Z} = \Lambda(\mathcal{Z},\mathfrak{t}), \quad 1 \geq \alpha > 0, \quad T_2 < \mathfrak{t} \leq T_3, \tag{41}$$

$$\mathcal{Z}(\mathfrak{t}_2) = \mathcal{Z}_2,$$

$$d\mathcal{Z} = \Upsilon(\mathcal{Z},\mathfrak{t})dB(\mathfrak{t}) + \Lambda(\mathcal{Z},\mathfrak{t})d\mathfrak{t}, \quad T_f \geq \mathfrak{t} > T_3, \tag{42}$$

$$\mathcal{Z}_3 = \mathcal{Z}(\mathfrak{t}_3).$$

Now, to solve (39) as follows [11]:

$$\mathcal{Z}^{k+1} = \mathcal{Z}^{k} + \frac{1-\alpha}{\mathcal{M}(\alpha)} - \left[\Lambda(\mathcal{Z}^{k},\mathfrak{t}^{k}) - \Lambda(\mathcal{Z}^{(k-1)},\mathfrak{t}^{(k-1)})\right] + \frac{\alpha}{\mathcal{M}(\alpha)}\left[\Lambda(\mathcal{Z}^{k},\mathfrak{t}^{k})\frac{3}{2}\Delta\mathfrak{t} - \Lambda(\mathcal{Z}^{(k-1)},\mathfrak{t}^{(k-1)})\frac{1}{2}\Delta\mathfrak{t}\right].$$

To solve (40) as follows [10]:

$$\mathcal{Z}^{\mathfrak{n}+1} = \frac{1}{(gg+gg1)}\left(gg1\sum_{i=k+1}^{\mathfrak{n}+1}\mu_i\mathcal{Z}^{\mathfrak{n}+1-i} - \mathfrak{q}_{\mathfrak{n}+1}\mathbb{Z}_0 - gg\sum_{i=k+1}^{\mathfrak{n}+1}\omega_i\mathcal{Z}^{\mathfrak{n}+1-i} - (\Lambda(\mathcal{Z}^{\mathfrak{n}},\mathfrak{t}^{\mathfrak{n}}))\right),$$

$$gg = \frac{\mathcal{G}_1(\alpha)}{\Theta(\Delta\mathfrak{t})^{\alpha-1}},$$

and

$$gg1 = \frac{\mathcal{G}_0(\alpha)}{\Theta(\Delta\mathfrak{t})^{\alpha}}.$$

To solve (41) as follows [11]:

$$\mathcal{Z}^{\mathfrak{n}_1+1} = \mathcal{Z}_0 + \frac{(1-\alpha)}{\mathcal{AB}(\alpha)}\left[\Lambda(\mathcal{Z}^{\mathfrak{n}_1},\mathfrak{t}^{\mathfrak{n}_1})\right] + \frac{\alpha(\Delta\mathfrak{t})^{\alpha}}{\mathcal{AB}(\alpha)\Gamma(\alpha+2)}\sum_{\mathfrak{h}=\mathfrak{n}+1}^{\mathfrak{n}_1}\Lambda(\mathcal{Z}^{\mathfrak{h}},\mathfrak{t}^{\mathfrak{h}})\Big[(\mathfrak{n}_1+1-\mathfrak{m})^{\alpha}(\mathfrak{n}_1+2-\mathfrak{h}+\alpha)$$

$$- (k-\mathfrak{m})^{\alpha}(k-\mathfrak{h}+2+2\alpha)\Big]$$
$$- \frac{\alpha(\Delta \mathfrak{t})^{\alpha}}{\mathcal{AB}(\alpha)\Gamma(\alpha+2)} \sum_{\mathfrak{h}=\mathfrak{n}+1}^{\mathfrak{n}_1} \Lambda(\mathcal{Z}^{(\mathfrak{h}-1)}, \mathfrak{t}^{(-1+\mathfrak{h})})\Big[(\mathfrak{n}_1-\mathfrak{h}+1)^{1+\alpha} - (\mathfrak{n}_1-\mathfrak{h})^{\alpha}(\mathfrak{n}_1+1-\mathfrak{h}+\alpha)\Big]. \tag{43}$$

To solve (42), we use the Milstein method as follows:

$$\mathcal{Z}^{(\mathfrak{n}_2+1)} = \mathcal{Z}^{(\mathfrak{n}_2)} + \Lambda(\mathcal{Z}^{\mathfrak{n}_2}, \mathfrak{t}^{\mathfrak{n}_2})\Delta\mathfrak{t} + \Upsilon(\mathcal{Z}^{(\mathfrak{n}_2)}, \mathfrak{t}^{(\mathfrak{n}_2)})\Delta B + 0.5\Upsilon(\mathcal{Z}^{(\mathfrak{n}_2)}, \mathfrak{t}^{(\mathfrak{n}_2)})\Upsilon'(\mathcal{Z}^{(\mathfrak{n}_2)}, \mathfrak{t}^{(\mathfrak{n}_2)})$$
$$((\Delta B_{\mathfrak{n}_2} - \Delta\mathfrak{t}). \tag{44}$$

$\mathfrak{n}_2 = \mathfrak{n}_1 + 1, \ldots, N.$

6 Discussion and Numerical Simulations

This section aims to validate the experimental results and analytical expressions derived in the previous sections. We utilize real-world data on cholera infections in Yemen, recorded between 27 April 2017, and 15 April 2018 [18]. The parameters and initial conditions used for the numerical simulations are outlined in Table 1.

All computations were performed using MATLAB 2021b on a PC equipped with an Intel(R) Core i7-3110M CPU (1.80 GHz) and 8 GB of RAM.

The numerical results for the proposed piecewise model are presented graphically:

- Fig. 1 illustrates a comparison between our numerical results and the actual data on cholera cases in Yemen. In this figure, we set $\alpha = 1$ and $\sigma_1 = \sigma_2 = \sigma_3 = \sigma_4 = \sigma_5 = 0$. The results demonstrate excellent alignment with previous studies, such as [3,5].
- Figs. 2–5 depict various scenarios comparing the simulated number of infected individuals to the real data. The numerical approximations closely match the observed cases, reinforcing the effectiveness of the proposed crossover model in accurately describing the spread of cholera in Yemen. Notably, our results surpass the accuracy of prior models presented in [3,5].
- Figs. 6 and 7 illustrate the influence of varying α on the solution's behavior, maintaining $\sigma_1 = \sigma_2 = \sigma_3 = \sigma_4 = \sigma_5 = 0$. The patterns observed are consistent with those reported in [5], indicating that the proposed model can reproduce outcomes from previous studies as a particular case.
- Fig. 8 reveals new dynamic behaviors under different values of α. The results highlight diverse solution patterns, suggesting that the disease exhibits multiple dynamic pathways. This observation underscores the importance of analyzing and predicting the progression of cholera from outbreak onset to resolution, capturing a range of behaviors from deterministic crossovers to stochastic fluctuations.

Overall, the proposed crossover model provides a robust and accurate framework for simulating the spread of cholera in Yemen, offering deeper insights into the complexity of infectious disease dynamics and surpassing the predictive capabilities of earlier models.

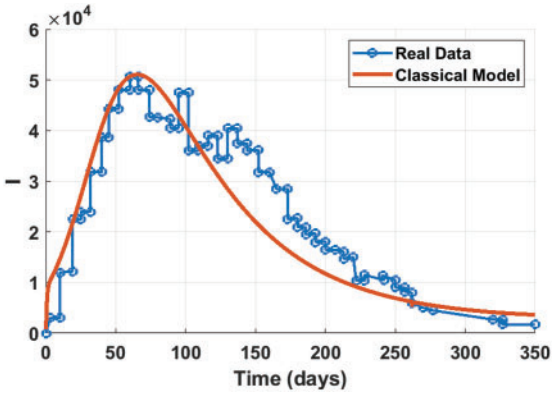

Figure 1: A comparison between real data and the classical model of cholera

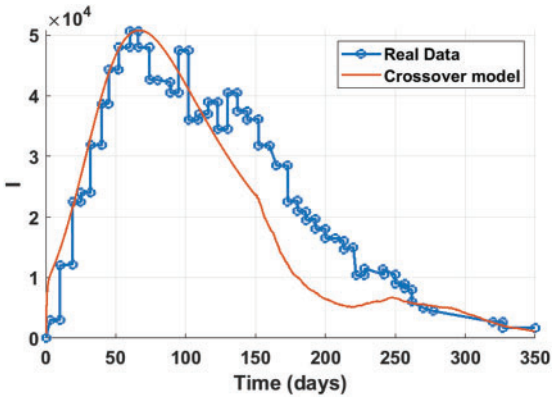

Figure 2: A comparison between real data and the classical model of cholera and $\alpha = 0.99$; $\sigma_1 = \sigma_2 = \sigma_3 = \sigma_4 = 0.01$, $\sigma_5 = 0$

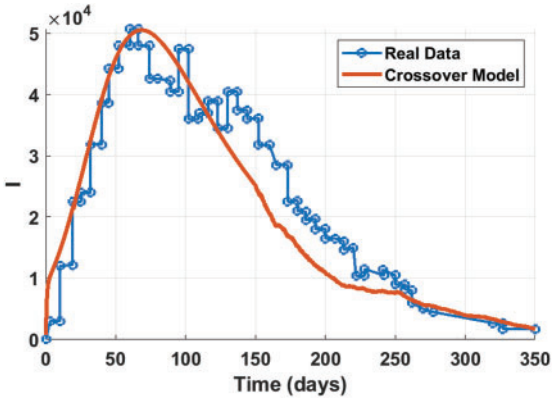

Figure 3: A comparison between real data and the classical model of cholera and $\alpha = 0.98$; $\sigma_1 = \sigma_2 = \sigma_3 = \sigma_4 = 0.01$, $\sigma_5 = 0$

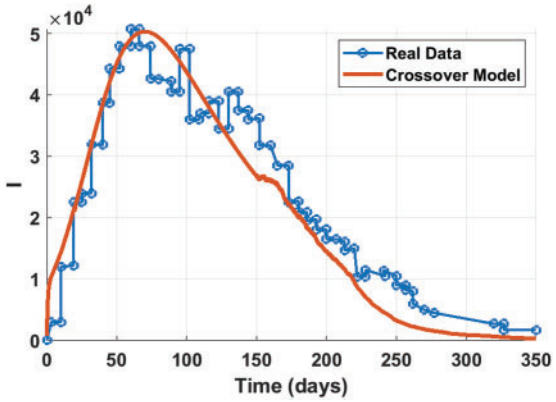

Figure 4: A comparison between real data and the classical model of cholera and $\alpha = 0.97$; $\sigma_1 = \sigma_2 = \sigma_3 = \sigma_4 = 0.01$, $\sigma_5 = 0$

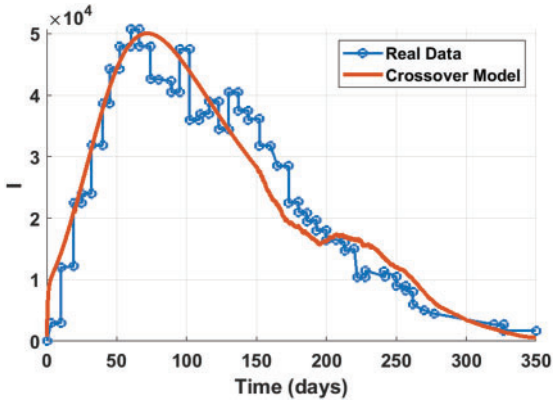

Figure 5: A comparison between real data and the classical model of cholera and $\alpha = 0.96$; $\sigma_1 = \sigma_2 = \sigma_3 = \sigma_4 = 0.01$, $\sigma_5 = 0$

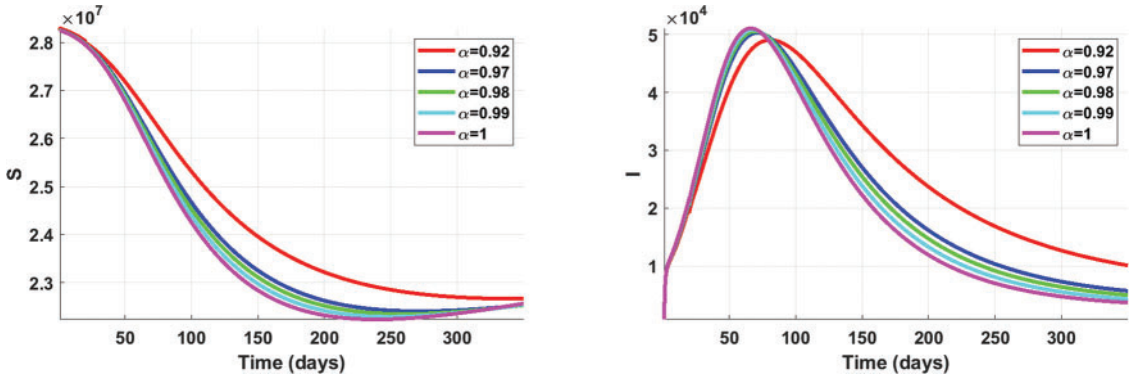

Figure 6: (Continued)

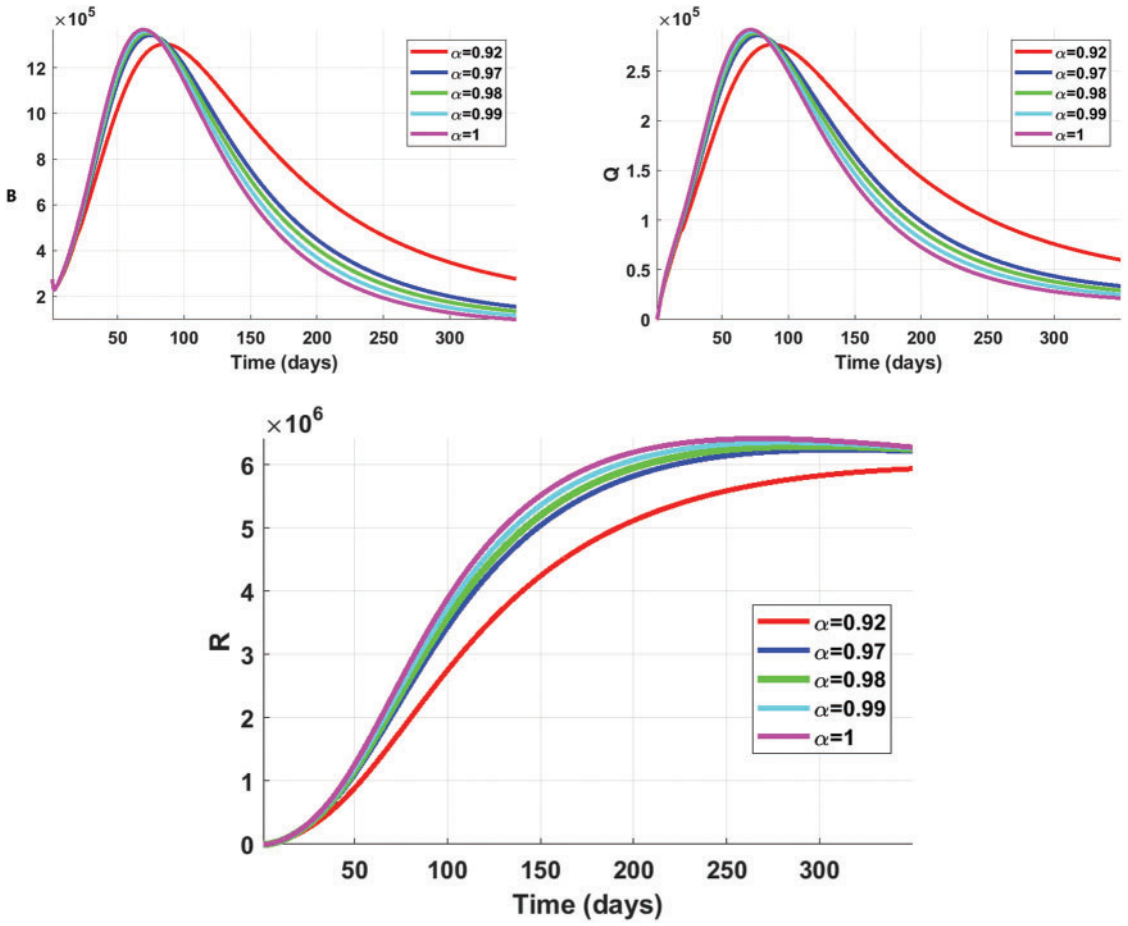

Figure 6: Numerical behavior of the proposed model at different values of α and $\sigma_1 = \sigma_2 = \sigma_3 = \sigma_4 = \sigma_5 = 0$

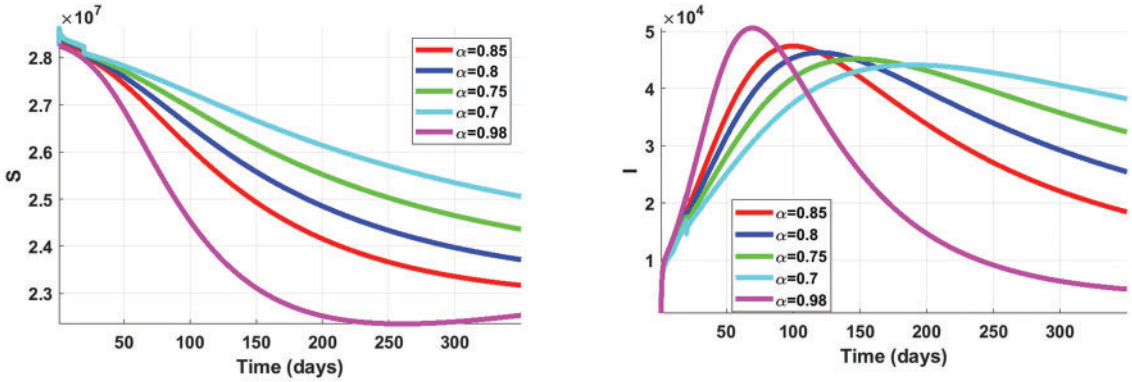

Figure 7: (Continued)

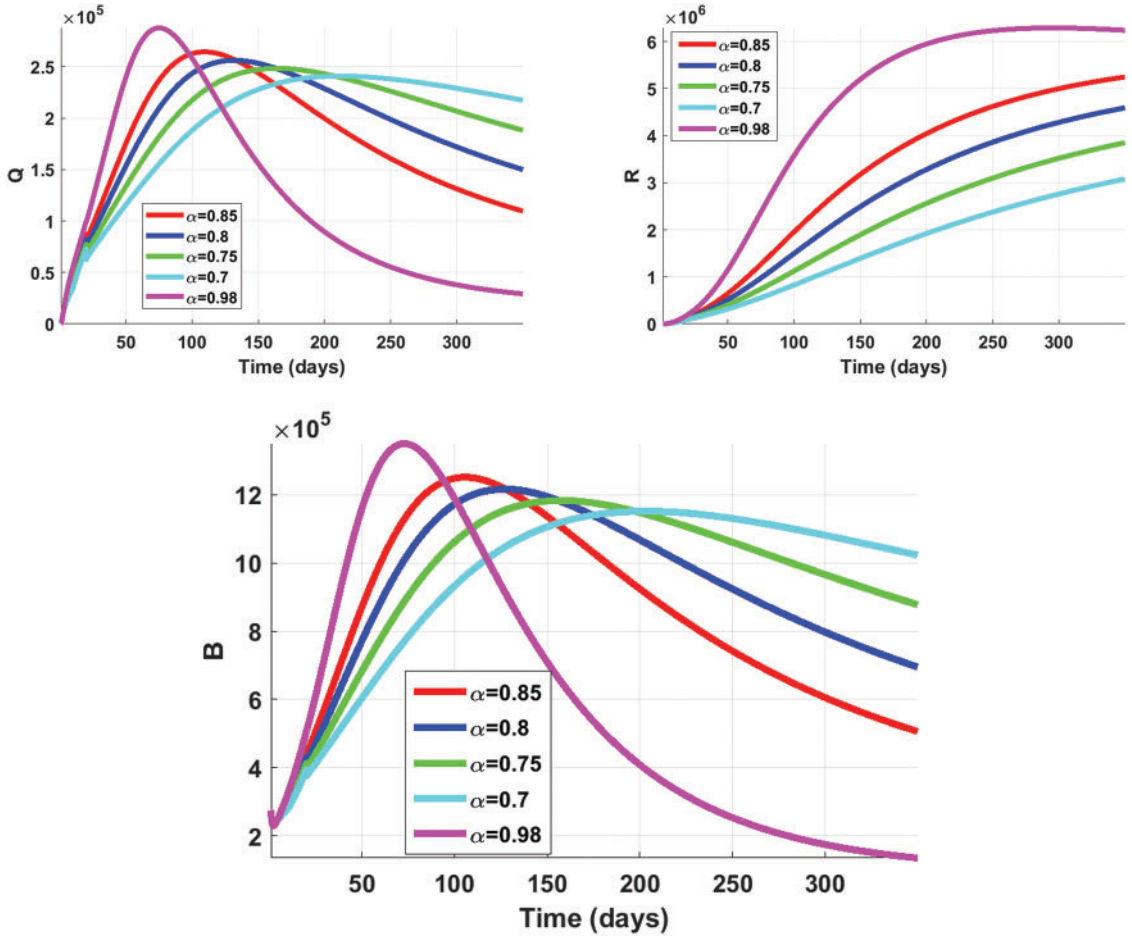

Figure 7: Numerical behavior of the proposed model at different values of α and $\sigma_1 = \sigma_2 = \sigma_3 = \sigma_4 = \sigma_5 = 0$

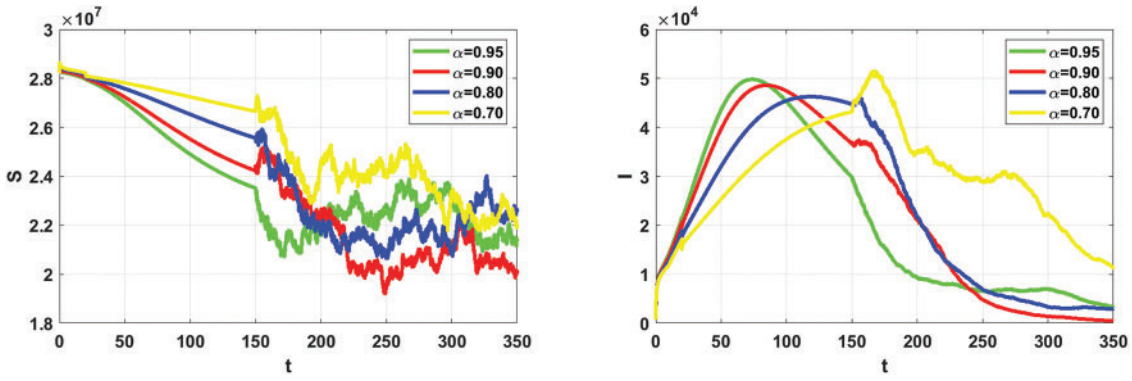

Figure 8: (Continued)

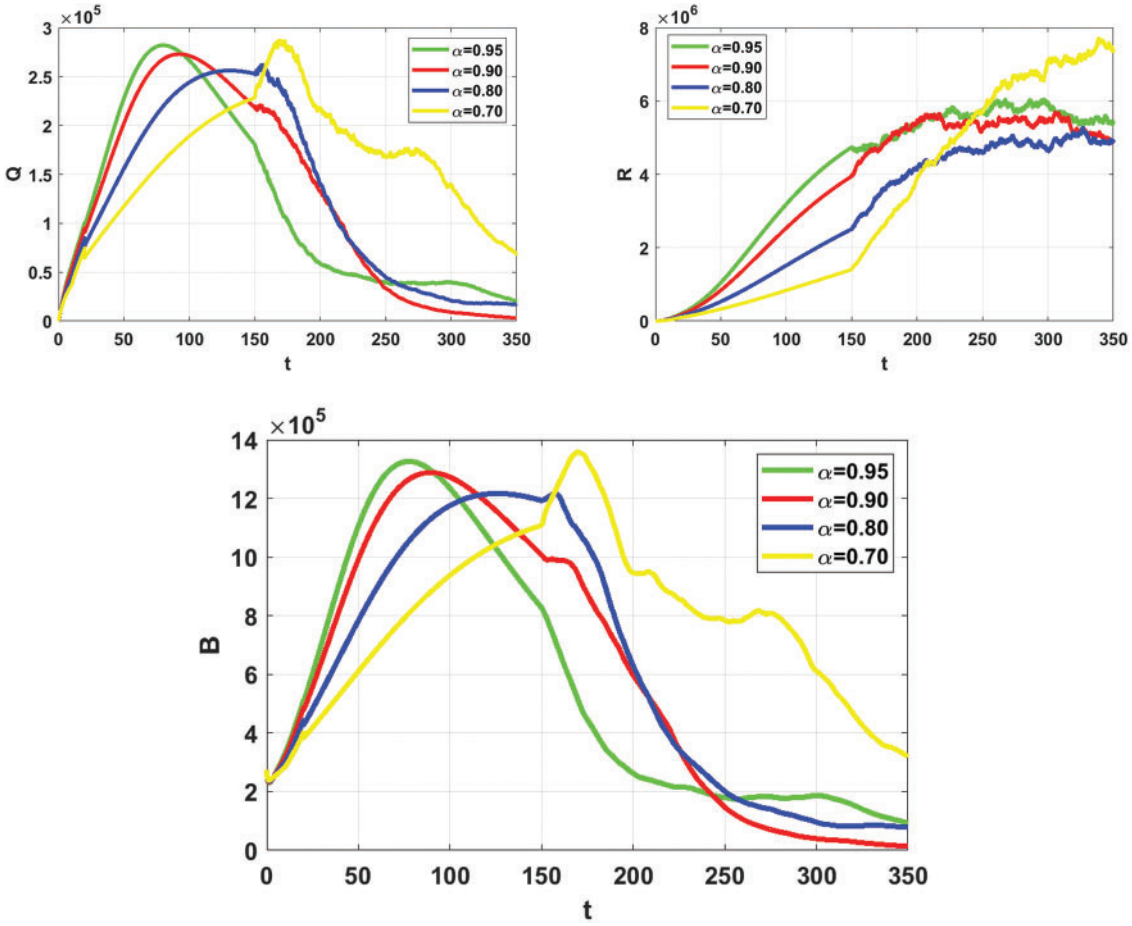

Figure 8: Numerical behavior of the proposed model at different values of α and $\sigma_1 = 0.01$, $\sigma_2 = 0.01$, $\sigma_3 = 0.01$, $\sigma_4 = 0.01$, $\sigma_5 = 0.0$

7 Conclusions

This study refined the mathematical model of cholera by incorporating a novel crossover framework. We integrated three distinct fractional derivatives—Caputo Fabrizio, Caputo proportional, and Atangana-Baleanu with SDEs to simulate the dynamics of the disease over four time intervals.

We employed CPC-GLNFDM for the numerical approximation of models with singular kernels, the Toufik-Atangana method for models with the Mittag-Leffler kernel, and the Milstein method for the SDEs. The stability of the proposed model was rigorously analyzed.

The results, validated against real data on cholera infections in Yemen from 27th April 2017, to 15 th April 2018, demonstrate that our model provides a more accurate approximation of the solution compared to previous studies. The integration of SDEs has significantly enhanced our understanding of the inherent randomness in infectious disease transmission, revealing diverse dynamic behaviors. This approach enables us to forecast disease trajectories from outbreak to resolution, capturing a broad spectrum of scenarios from deterministic crossovers to stochastic processes.

Piecewise crossover differential equations, combining fractional and stochastic elements, offer a powerful framework for modeling complex systems with time-varying dynamics. This approach has the potential to enhance our ability to model and predict the behavior of various real-world phenomena accurately.

Future research will focus on expanding the model to incorporate spatial heterogeneity and mobility patterns, which play a critical role in the spread of infectious diseases. Investigating the application of machine learning techniques to optimize parameter estimation and enhance predictive accuracy is another promising avenue. Additionally, we plan to apply this crossover modeling framework to other infectious diseases and environmental phenomena, aiming to uncover universal patterns in dynamic systems. Further exploration of multi-scale modeling, integrating micro and macro-level interactions, will provide deeper insights into disease dynamics and control strategies.

Acknowledgement: The authors wish to express sincere appreciation to the reviewers for their valuable comments, which significantly improved this paper.

Funding Statement: The authors received no specific funding for this study.

Author Contributions: The authors confirm their contribution to the paper as follows: Conceptualization, formal analysis, resources, software, supervision, writing—original draft, methodology, validation, writing—original draft, data collection: Seham M. Al-Mekhlafi. Conceptualization, supervision, visualization, resources: Kamal R. Raslan, Khalid K. Ali. Writing—original draft, methodology, data collection: Sadam H. Alssad. Funding acquisition, resources, visualization: Nehaya R. Alsenaideh. All authors reviewed the results and approved the final version of the manuscript.

Availability of Data and Materials: The data that support the findings of this study are available from the first and corresponding author upon reasonable request.

Ethics Approval: Not applicable.

Conflicts of Interest: The authors declare no conflicts of interest to report regarding the present study.

References

1. Ali M, Nelson AR, Lopez AL, Sack DA. Updated global burden of cholera in endemic countries. PLoS Negl Trop Dis. 2015;9(6):e0003832. doi:10.1371/journal.pntd.0003832.
2. Huppert A, Katriel G. Mathematical modelling and prediction in infectious disease epidemiology. Clin Microbiol Infect. 2013;19(11):999–1005. doi:10.1111/1469-0691.12308.
3. Lemos-Paião AP, Silva1 CJ, Torres DFM, Venturino E. Optimal control of aquatic diseases: a case study of Yemen's cholera outbreak. J Optim Theory Appl. 2020;185(3):1008–30. doi:10.1007/s10957-020-01668-z.
4. Lemos-Paião AP, Silva CJ, Torres DFM. An epidemic model for cholera with optimal control treatment. J Comput Appl Math. 2017;318(1):168–80. doi:10.1016/j.cam.2016.11.002.
5. Baleanu D, Ghassabzade FA, Nieto JJ, Jajarmi A. On a new and generalized fractional model for the real cholera outbreak. Alex Eng J. 2022;61(11):9175–86. doi:10.1016/j.aej.2022.02.054.
6. Singh H, Srivastava HM, Pandey RK. Special functions in fractional calculus and engineering. Boca Raton: CRC Press; 2023.
7. Caputo M, Fabrizio M. A new definition of fractional derivative without singular kernel. Prog Fract Differ Appl. 2015;1(2):73–85.
8. Baleanu D, Fernandez A, Akgül A. On a fractional operator combining proportional and classical differintegrals. Mathematics. 2020;8(3):360. doi:10.3390/math8030360.
9. Atangana A, Baleanu D. New fractional derivatives with non-local and non-singular kernel: theory and application to heat transfer model. Therm Sci. 2016;20(2):763–9.
10. Sweilam H, Al-Mekhlafi SM, Abou Hasan MM, Soliman T. New crossover lumpy skin disease: numerical treatments. Partial Differential Equations in Applied Mathematics. 2024;12(4):100986. doi:10.1016/j.padiff.2024.100986.
11. Atangana A, Araz S. New numerical scheme with Newton polynomial: theory, methods, and applications. London, UK: Academic Press; 2021.

12. Mil'shtein GN. Approximate integration of stochastic differential equations. Theor Probab Appl. 1974;19(3):583–8. (In Russian). doi:10.1137/1119062.
13. Podlubny I. Fractional differential equations. New York, NY, USA: Academic Press; 1999.
14. Van den Driessche P, Watmough J. Reproduction numbers and sub-threshold endemic equilibria for compartmental models of disease transmission. Math Biosci. 2002;180:29–48. doi:10.1016/S0025-5564(02)00108-6.
15. Hanif A, Butt AIK. Atangana-Baleanu fractional dynamics of dengue fever with optimal control strategies. AIMS Math. 2023;8(7):15499–535. doi:10.3934/math.2023791.
16. Scherer R, Kalla S, Tang Y, Huang J. The Grünwald-Letnikov method for fractional differential equations. Comput Math Appl. 2011;62(3):902–17. doi:10.1016/j.camwa.2011.03.054.
17. Rihan FA, Lakshmanan S, Hashish AH, Rakkiyappan R, Ahmed E. Fractional-order delayed predator prey systems with Holling type-II functional response. Nonlinear Dyn. 2015;80:777–89. doi:10.1007/s11071-015-1905-8.
18. World Health Organization. Yemen: weekly cholera bulletins. [cited 2025 May 5]. Available from: https://www.who.int/emergencies/disease-outbreak-news/item/yemen-cholera.